LETTER

https://doi.org/10.1038/s41586-018-0729-3

Mannose impairs tumour growth and enhances chemotherapy

Pablo Sierra Gonzalez[1], James O'Prey[1], Simone Cardaci[1,2,6], Valentin J. A. Barthet[1,6], Jun-ichi Sakamaki[1], Florian Beaumatin[1], Antonia Roseweir[3], David M. Gay[1], Gillian Mackay[1], Gaurav Malviya[1], Elżbieta Kania[1], Shona Ritchie[1], Alice D. Baudot[1], Barbara Zunino[1], Agata Mrowinska[1], Colin Nixon[1], Darren Ennis[3,5], Aoisha Hoyle[4], David Millan[4], Iain A. McNeish[3,5], Owen J. Sansom[1,3], Joanne Edwards[3] & Kevin M. Ryan[1,3]*

It is now well established that tumours undergo changes in cellular metabolism[1]. As this can reveal tumour cell vulnerabilities and because many tumours exhibit enhanced glucose uptake[2], we have been interested in how tumour cells respond to different forms of sugar. Here we report that the monosaccharide mannose causes growth retardation in several tumour types in vitro, and enhances cell death in response to major forms of chemotherapy. We then show that these effects also occur in vivo in mice following the oral administration of mannose, without significantly affecting the weight and health of the animals. Mechanistically, mannose is taken up by the same transporter(s) as glucose[3] but accumulates as mannose-6-phosphate in cells, and this impairs the further metabolism of glucose in glycolysis, the tricarboxylic acid cycle, the pentose phosphate pathway and glycan synthesis. As a result, the administration of mannose in combination with conventional chemotherapy affects levels of anti-apoptotic proteins of the Bcl-2 family, leading to sensitization to cell death. Finally we show that susceptibility to mannose is dependent on the levels of phosphomannose isomerase (PMI). Cells with low levels of PMI are sensitive to mannose, whereas cells with high levels are resistant, but can be made sensitive by RNA-interference-mediated depletion of the enzyme. In addition, we use tissue microarrays to show that PMI levels also vary greatly between different patients and different tumour types, indicating that PMI levels could be used as a biomarker to direct the successful administration of mannose. We consider that the administration of mannose could be a simple, safe and selective therapy in the treatment of cancer, and could be applicable to multiple tumour types.

As tumours often have a high avidity for glucose[4], we examined the effect of other sugars on the growth of tumour cells. This revealed that mannose, in contrast to other sugars, significantly reduced the growth of U2OS cells (Fig. 1a). Similar effects occurred in Saos-2 cells, with fucose also causing a comparatively small decrease in cell growth (Extended Data Fig. 1a). Using a panel of cell lines, we observed that this effect of mannose occurs in cells from various tissues, with the effect being greater in some cells than others (Fig. 1b, c, Extended Data Fig. 1a–d).

Mannose is imported into cells by means of the same transporters as glucose[3], so we considered that mannose might interfere with the uptake of glucose. In support of this hypothesis, we observed that mannose enhances levels of phosphorylated AMPK—a read-out of energy balance in cells[5,6] (Extended Data Fig. 1e). However, liquid chromatography coupled with mass spectrometry (LC–MS) analyses showed that levels of the phosphorylated form of the glucose analogue 2-deoxyglucose (2-DG-P)—used as a proxy for glucose uptake—did not correlate with mannose sensitivity in mannose-sensitive compared with mannose-insensitive cell lines (Fig. 1a, b, Extended Data Fig. 1f, g). In fact, mannose increased the intracellular pool of hexose-6-phosphate, which is produced in the first step of the metabolism of glucose and mannose (Extended Data Fig. 1h). This effect was not observed with other sugars (Extended Data Fig. 1i).

To determine whether the mannose-induced increase in hexose-6-phosphate levels is due to mannose or glucose, we performed LC–MS with an extended chromatography time to enable selective detection of the unphosphorylated form of these sugars. This revealed that mannose increased the intracellular pool of mannose, as expected, but it also increased the intracellular pool of glucose (Extended Data Fig. 1j, k). To corroborate this finding, we treated cells with glucose labelled with two atoms of ^{13}C (1,2-$^{13}C_2$-glucose) and mannose labelled with six atoms of ^{13}C ($^{13}C_6$-mannose) to enable detection due to differences in molecular mass; we again found that treatment with mannose increased intracellular levels of glucose (Extended Data Fig. 1l).

As mannose did not reduce intracellular levels of glucose, but significantly affected cell growth, we considered that it might interfere with glucose metabolism. There is considerable crosstalk between the metabolism of these sugars, and mannose-6-phosphate can inhibit three enzymes that mediate glucose metabolism: hexokinases, phosphoglucose isomerase (PGI) and glucose-6-phosphate dehydrogenase[7] (Fig. 1d). To address this possibility, we measured the levels of hexose-6-phosphate and lactate when cells were incubated in glucose-free medium supplemented with either 1,2-$^{13}C_2$-glucose or $^{13}C_6$-mannose. This revealed that mannose accounts for more of the mannose-induced hexose-6-phosphate accumulation than does glucose, but also that glucose-6-phosphate is produced in the presence of mannose, albeit at lower levels when compared with cells treated with glucose alone (Fig. 1e). We also observed that mannose produces only small amounts of lactate—indicating that it is poorly metabolised—and more notably, mannose markedly reduces the production of lactate from glucose (Fig. 1f). Further analysis revealed that mannose treatment not only affects pools of glycolytic intermediates, but also affects those involved in the tricarboxylic acid cycle, the pentose phosphate pathway and glycan synthesis (Fig. 1g–i). As with the effects on cell growth, these metabolic effects were not observed to the same extent with other sugars (Extended Data Fig. 1m–p). Moreover, although mannose uptake was not lower in mannose-insensitive cells when compared to mannose-sensitive cells (Extended Data Fig. 2a), the effects of mannose on metabolism were only observed in cells sensitive to the sugar (Extended Data Fig. 2b–h). We also found that mannose-induced AMPK phosphorylation does not occur concomitantly with changes in the levels of AMP or ATP, but is associated with a decrease in fructose-1,6-bisphosphate levels, as has been recently described[6] (Extended Data Fig. 3a–f).

Because mannose affects the growth of tumour cells, we questioned whether it can also affect the cellular response to chemotherapeutic drugs. Although mannose alone did not affect cell viability, it significantly enhanced cell death when administered with cisplatin or doxorubicin—an effect not seen with other hexoses (Fig. 2a, b,

[1]Cancer Research UK Beatson Institute, Glasgow, UK. [2]Division of Genetics and Cell Biology, San Raffaele Scientific Institute, Milan, Italy. [3]Institute of Cancer Sciences, University of Glasgow, Glasgow, UK. [4]Department of Pathology, Queen Elizabeth University Hospital, Glasgow, UK. [5]Present address: Department of Surgery and Cancer, Imperial College London, London, UK. [6]These authors contributed equally: Simone Cardaci, Valentin J. A. Barthet. *e-mail: k.ryan@beatson.gla.ac.uk

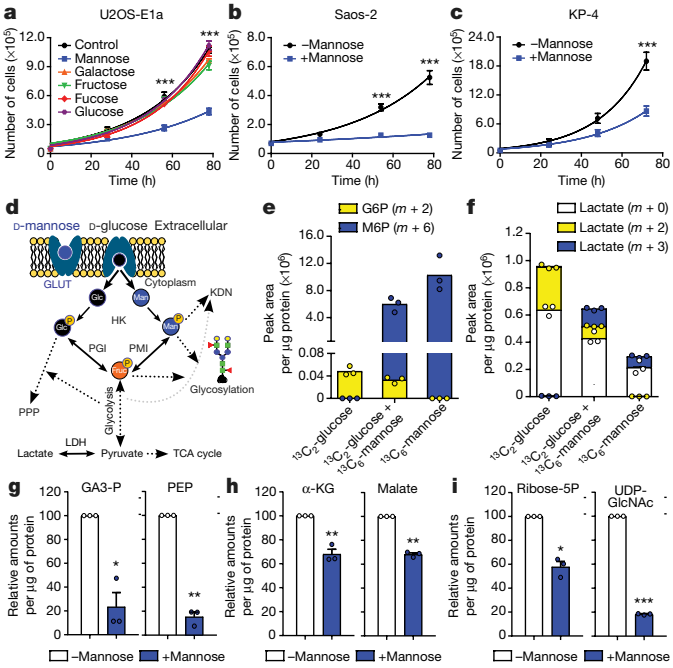

Fig. 1 | Mannose impairs the growth of cancer cells and interferes with glucose metabolism by accumulating intracellularly as mannose-6-phosphate. a, Growth curves of U2OS-E1a cells supplemented without (control) or with 25 mM of the hexoses stated. **b**, **c**, Growth curves of Saos-2 cells in DMEM alone (−mannose) or DMEM with an additional 25 mM mannose (+mannose) (**b**) and KP-4 cells in IMDM alone or with 25 mM mannose (**c**). **d**, Scheme of mannose metabolism: mannose enters the cells using the same transporters as glucose (GLUT) and is phosphorylated into mannose-6-phosphate by hexokinases (HK). Mannose can then be used for glycosylation purposes or isomerized into fructose-6-phosphate by PMI; both PMI and PGI can also produce mannose-6-phosphate from glucose-6-phosphate. Mannose-6-phosphate also participates in the biosynthesis of deaminoneuraminic acid (KDN). Fruc, fructose; glc, glucose; man, mannose; TCA cycle, tricarboxylic acid cycle. **e**, **f**, Extraction of intracellular metabolites and measurement of the peak area per microgram of protein of glucose-6-phosphate (G6P) ($m + 2$) and mannose-6-phosphate (M6P) ($m + 6$) (**e**) and lactate ($m + 0$, $m + 2$, $m + 3$) (**f**), after 6-h incubation of U2OS-E1a cells in 10% dialysed FBS in glucose-free DMEM complete medium in the presence of 5 mM 1,2-$^{13}C_2$-D-glucose alone, 5 mM $^{13}C_6$-D-mannose alone, or both sugars in combination. **g**–**i**, Relative amounts per microgram of protein of the intracellular metabolites glyceraldehyde-3-phosphate (GA3-P) (left) and phosphoenolpyruvate (PEP) (right) (**g**); α-ketoglutarate (α-KG) (left) and malate (right) (**h**); ribose-5-phosphate (ribose-5P) (left) and UDP-*N*-acetyl-glucosamine (UDP-GlcNAc) (right) (**i**) after a 6-h incubation of U2OS-E1a cells in 10% dialysed FBS in DMEM complete medium with 5 mM glucose, with or without 5 mM mannose as indicated. $n = 3$ independent experiments (**a**–**c**, **g**–**i**); data are representative of three independent experiments (**e**, **f**). Data are mean ± s.e.m. and were analysed by two-way ANOVA with Bonferroni correction (**a**–**c**) or paired two-tailed Student's *t*-test (**g**–**i**). $*P < 0.05$, $**P < 0.01$, $***P < 0.001$.

Extended Data Fig. 4a–c). Mechanistically, the combination of mannose and the chemotherapeutic drug increased the levels of cleaved poly(ADP-ribose) polymerase (PARP, a substrate[8] of caspase-3) and this effect, together with cell death, was blocked by the pan-caspase inhibitor zVAD-FMK (Fig. 2c, d, Extended Data Fig. 4d).

Because our data indicated that cell death after treatment with mannose and the chemotherapeutic drug is likely to proceed by apoptosis, we used CRISPR–Cas9 to determine which apoptotic pathways might be involved. Disruption of caspase 8 and FADD—two components of the extrinsic apoptotic pathway[9]—had no effect on cell death (Extended Data Fig. 4e–g). By contrast, disruption of Bax and Bak—essential factors for mitochondrial outer membrane permeabilization and the intrinsic pathway[10]—markedly reduced cell death after treatment with mannose in combination with either cisplatin or doxorubicin (Fig. 2e, Extended Data Fig. 4h, i).

As mitochondrial outer membrane permeabilization is controlled by members of the Bcl-2 family[11], we examined the levels of these proteins in the presence of mannose, cisplatin or both in combination. In agreement with previous studies that detail a role for the Noxa/Mcl-1 axis in cell death induced by glycolysis inhibition and glucose deprivation[12–14], we found that levels of Noxa increased after treatment with cisplatin and cisplatin plus mannose, and levels of Mcl-1 and Bcl-X_L decreased after the combination treatment (Fig. 2f, Extended Data Fig. 4j). Mechanistically, we consider that the change in Mcl-1 and Bcl-X_L levels is due to decreased translation because the levels of the proteins themselves were still decreased in the presence of a proteasome inhibitor, and there was no change in the levels of their mRNAs, after the combination treatment (Extended Data Fig. 4k–m). The involvement of these proteins was confirmed by CRISPR-mediated disruption of *PMAIP1* (also known as *NOXA*) or by overexpression of Mcl-1 or Bcl-X_L, which all suppressed cell death induced by mannose and chemotherapy (Fig. 2g, h, Extended Data Figs. 4n–q, 5a). Finally, we also observed that mannose enhances cell death induced by the Bcl-X_L antagonist WEHI539, but not the Bcl-2 antagonist ABT-199 (Extended Data Fig. 5b).

We were keen to find out whether mannose also has effects in vivo. Tumour-bearing mice were given a single oral gavage of mannose, which resulted in a serum concentration of approximately 3 mM (Extended Data Fig. 6a). Mice were then injected with 2-deoxy-2-[^{18}F]fluoro-D-glucose ([^{18}F]FDG) to monitor [^{18}F]FDG uptake and its subsequent conversion by hexokinases into [^{18}F]FDG-6-phosphate[15]. As mannose impedes hexokinases[6], we found that the [^{18}F]FDG signal (provided by [^{18}F]FDG and/or [^{18}F]FDG-6-phosphate) was significantly reduced in mannose-treated mice when compared with control mice bearing tumours of an equivalent size (Fig. 3a, Extended Data Fig. 6b, c). A significant effect of mannose treatment on the [^{18}F]FDG signal was also seen in certain normal tissues (Extended Data Fig. 6d).

To test whether mannose could affect tumour growth, mice were injected with tumour cells subcutaneously and were given mannose both freely in drinking water and three times a week by oral gavage. This did not affect the weight of the mice, nor did it visibly affect their health (Extended Data Fig. 6e). However, it significantly inhibited tumour growth (Fig. 3b), involving decreased numbers of BrdU-positive cells, which indicates that mannose inhibits cell proliferation both in vitro and in vivo (Extended Data Fig. 6f, g).

We were also interested to know whether mannose can enhance chemotherapy in vivo. Tumour-bearing nude mice were treated with mannose and doxorubicin either alone or in combination. Although none of the treatments affected the weight or visibly affected the health of the mice (Extended Data Fig. 6h), we found that either doxorubicin or mannose caused a reduction in tumour volume (Fig. 3c). Moreover, an even greater effect was observed when doxorubicin was administered in combination with mannose (Fig. 3c). Notably, when we examined the overall survival of the treated cohorts, those treated with doxorubicin plus mannose had a significantly increased life expectancy when compared to untreated mice or those treated with either doxorubicin or mannose alone (Fig. 3d).

As our data indicated that mannose could potentially be used clinically, we wanted to understand why different cells vary in their sensitivity to the sugar. Because mannose affects several metabolic pathways, we reasoned that sensitivity may be connected to an apical enzyme involved in sugar metabolism. Our profiling revealed that mannose sensitivity was roughly inversely correlated with the levels and activity of PMI, the enzyme that catalyses the interconversion of mannose-6-phosphate and fructose-6-phosphate[16] (Figs. 1a–c and 4a, Extended Data Figs. 1b–d, f, 7a). Consequently, we knocked down *MPI*, the gene that encodes PMI, in three mannose-insensitive cell lines: SKOV3, RKO and IGROV1. In each case, *MPI* knockdown caused growth retardation upon mannose treatment (Fig. 4b, Extended Data Fig. 7b–g) and markedly sensitized cells to cell death when mannose

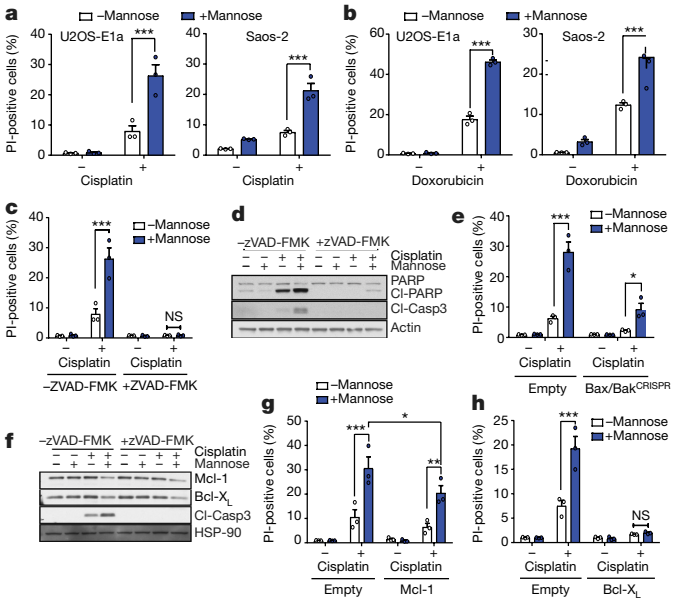

Fig. 2 | The combination of chemotherapeutic drugs with mannose enhances cell death by potentiating the intrinsic pathway of apoptosis through the downregulation of Mcl-1 and Bcl-X_L protein levels. **a**–**h**, All experiments were performed by pre-incubating cells in the presence of complete DMEM or complete DMEM supplemented with 25 mM sugars for 24 h before the addition of other treatments. **a**, **b**, The percentage of U2OS-E1a (left) and Saos-2 (right) propidium-iodide (PI)-positive cells after 24 h treatment with 10 μM cisplatin (**a**) and 1 μg ml^{-1} of doxorubicin (**b**) in the presence or absence of 25 mM mannose as indicated. **c**, The percentage of U2OS-E1a propidium-iodide-positive cells treated for 24 h with or without 10 μM cisplatin, with or without 25 mM mannose and with or without 50 μM of the caspase inhibitor zVAD-FMK. **d**, Western blots showing the levels of cleaved PARP (Cl-PARP) and cleaved caspase-3 (Cl-Casp3) in U2OS-E1a cells after 24 h treatment with or without 10 μM cisplatin, with or without 25 mM mannose and with or without 50 μM zVAD-FMK. **e**, The percentage of empty (left) and Bax/Bak^{CRISPR} (right) U2OS-E1a propidium-iodide-positive cells treated with or without 10 μM cisplatin and with or without 25 mM mannose for 24 h. **f**, Western blots showing the levels of Mcl-1, Bcl-X_L and cleaved caspase-3 in U2OS-E1a cells after 24 h with or without 10 μM cisplatin, with or without 25 mM mannose and with or without 50 μM zVAD-FMK. **g**, **h**, Percentage of propidium-iodide-positive U2OS-E1a (empty, Mcl-1 and Bcl-X_L overexpressing) cells after 24 h treatment with or without 10 μM cisplatin and with or without 25 mM mannose. $n = 3$ independent experiments (**a**–**c**, **e**, **g**, **h**); data are representative of three independent experiments (**d**, **f**). Data are mean ± s.e.m. and were analysed by two-way ANOVA with Bonferroni correction (**a**–**c**, **e**, **g**, **h**). $^*P < 0.05$, $^{**}P < 0.01$, $^{***}P < 0.001$.

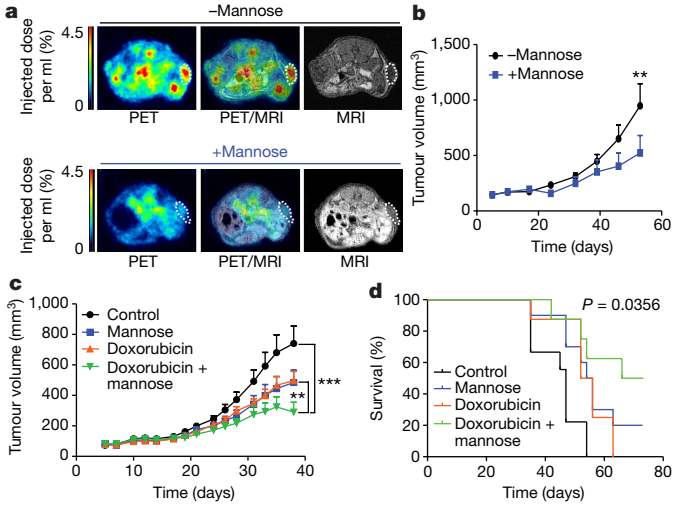

Fig. 3 | Mannose impairs tumour growth and induces tumour regression in combination with chemotherapy. **a**, CD1-nude mice were transplanted with KP-4 cells subcutaneously and tumours were grown for 14 days before positron emission tomography (PET) and magnetic resonance imaging (MRI) scans were carried out. **a**, PET and MRI scans of mice treated with 200 μl of water (top) or 200 μl of 20% (w/v) mannose in water (bottom) by oral gavage 20 min before injection of [^{18}F]FDG into the tail vein. White dotted circles highlight tumour areas in axial view of the mice. **b**, CD1-nude mice were injected with KP-4 cells subcutaneously and received either normal drinking water or 20% mannose in the drinking water, plus the same treatment (either normal water or 20% mannose) by oral gavage three days a week from the third day after tumour transplantation. Tumour volume (mm^3) was measured as indicated. **c**, **d**, CD1-nude mice were injected with KP-4 cells subcutaneously and tumours were grown for 10 days before the start of mannose treatment. Mice received either normal drinking water (control and doxorubicin) or 20% mannose in the drinking water (mannose and doxorubicin + mannose), plus the same treatment (either water or 20% mannose in water) via oral gavage three days a week. Doxorubicin treatment started on day 32 and mice received 5 mg kg^{-1} by intraperitoneal injection once a week. **c**, Tumour volume (mm^3) of all treatment groups. **d**, Graph representing the survival of the mice in all treatment groups until the end of the experiment at day 73. The number of mice for each experiment is as follows: $n = 5$ (−mannose), $n = 4$ (+mannose) (**a**); $n = 10$ (−mannose), $n = 8$ (+mannose) (**b**); $n = 10$ per group (**c**, **d**). Data are mean ± s.e.m. and were analysed by two-way ANOVA with Bonferroni correction (**b**, **c**) or log-rank test (two-sided Mantel–Cox test) (**d**). $^{**}P < 0.01$, $^{***}P < 0.001$.

was administered together with cisplatin (Fig. 4c). Conversely, the overexpression of *MPI* in a mannose-sensitive cell line rendered the cell line refractory to the effects of mannose on both cell growth and cell death (Fig. 4d, Extended Data Fig. 7h–k). Finally, we found that mannose treatment following *MPI* knockdown had highly significant effects on metabolic pathways downstream of the sugar (Fig. 4e, Extended Data Fig. 7l–o).

We next questioned whether PMI could be modulated to affect the response of tumours to mannose in vivo. As the immune microenvironment is important in many therapeutic situations and because mannose can affect immune cell function[17,18], we decided to use immune-competent mice and two syngeneic cell lines (B16-F1 and LLC) that are ordinarily mannose-insensitive but become mannose-sensitive upon *Mpi* knockdown (Fig. 4f, g, Extended Data Fig. 8a–d). In both cases, allografts formed with *Mpi*-knockdown cells were highly sensitive to the oral administration of mannose (Fig. 4h–k), without visibly affecting the health or weight of the mice (Extended Data Fig. 8e–h).

We were keen to know whether PMI levels varied in human tumours, such that the analysis of PMI could potentially be used as a biomarker for mannose sensitivity. We therefore stained tissue microarrays containing sections from ovarian, renal, breast, prostate and colorectal cancers. This revealed that PMI levels not only varied among tumours from the same tissue, but also between tissues (Fig. 4l, Extended Data Fig. 9a). PMI levels did not, however, have prognostic significance in breast and colon cancer, presumably because normal serum levels of mannose are low compared to glucose[19] (Extended Data Fig. 9b–d).

Most notable from our analyses was the fact that colorectal tumours generally have very low PMI levels (Fig. 4l), which indicates that they may be broadly sensitive to mannose. To explore this, we used an inflammation-driven model of colorectal cancer and a genetically engineered mouse model driven by two genes that are frequently altered in this disease (*Kras* and *Apc*)[20]. In both models, mice maintained on drinking water containing 20% mannose had significantly fewer tumours at the clinical end point (Fig. 4m, n), and notably, mannose had no negative effect on the health or weight of the mice over the time examined (Extended Data Fig. 9e, f).

In contrast to its effects on glucose metabolism, mannose does not decrease the uptake of amino acids or fatty acids, and although mannose reduces glucose-dependent serine and glycine synthesis, this contributes only marginally to total cellular serine and glycine pools

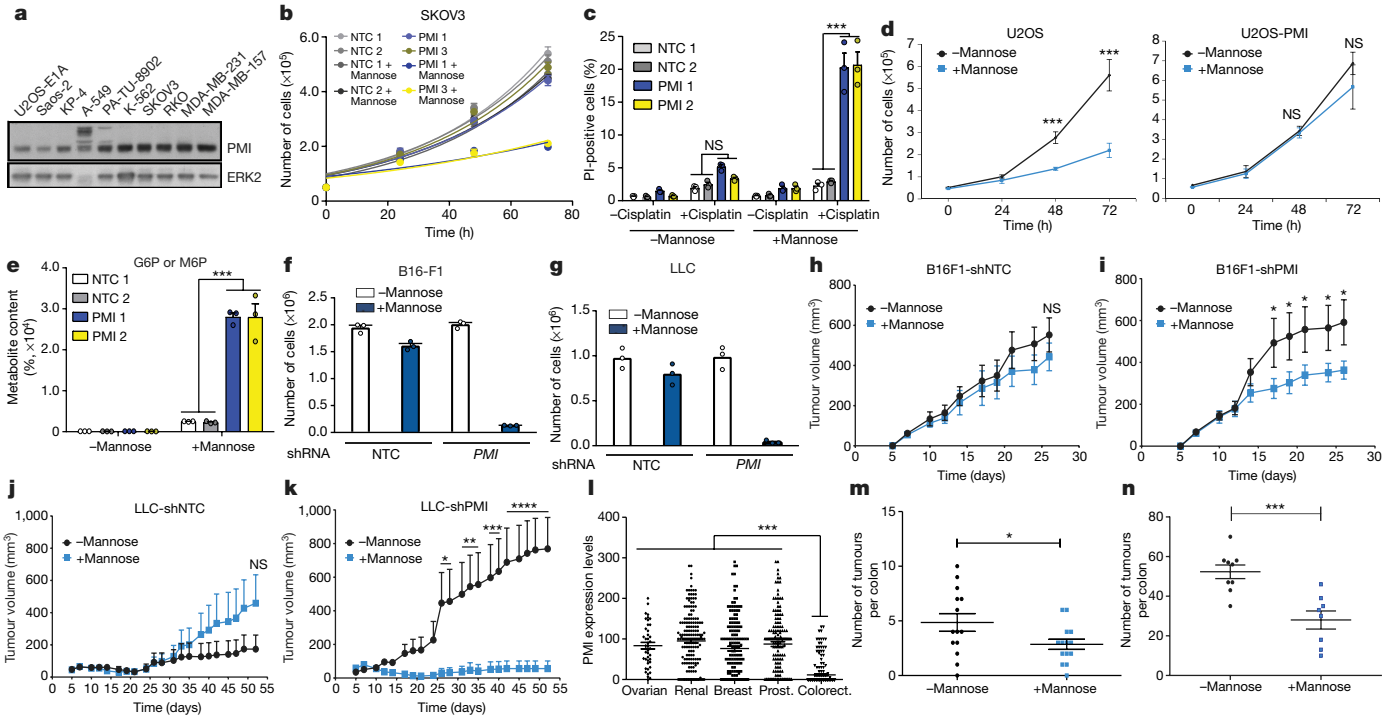

Fig. 4 | PMI levels dictate mannose sensitivity. a, Western blot showing the levels of PMI and ERK2 in a panel of ten cancer cell lines. **b**, Growth curves of SKOV3 cells in complete DMEM medium with or without supplementation of 25 mM mannose after transient transfection with two non-targeting (NTC) and two PMI-targeting short interfering RNAs (siRNAs) individually for 48 h. **c**, Cell death represented as the percentage of propidium-iodide-positive SKOV3 siRNA-transfected cells that had been pre-incubated with or without 25 mM mannose in regular DMEM for 24 h, before either 10 μM cisplatin was added or no cisplatin was added with incubation for a further 24 h. **d**, Overexpression of PMI renders U2OS-E1a insensitive to mannose. Growth curves of U2OS-E1a overexpressing PMI (U2OS-PMI) and U2OS-E1a cells expressing vector control (U2OS) after culture in either in DMEM or DMEM containing 25 mM mannose. **e**, Percentage of metabolite content of hexoses-6-phosphate in SKOV3 cells transfected with siRNA for 48 h before 6 h incubation in complete DMEM medium with or without supplementation of 25 mM mannose. Cells treated with NTC 1 without mannose were normalized to 100%. **f**, **g**, Knockdown of *Mpi* renders B16-F1 and LLC cells sensitive to mannose. The indicated cells were incubated with or without 25 mM mannose for 24 h before cell counting. **h**–**k**, B16-F1 or LLC cells expressing *Mpi*-targeting or control shRNAs were injected into the flanks of C57BL/6 mice. Mice were maintained either with or without 20% mannose in drinking water and tumour growth was monitored over time ($n = 10$ mice per group). **l**, *MPI* expression levels in tissue microarrays from ovarian ($n = 45$), renal ($n = 180$), breast ($n = 159$), prostate (prost.) ($n = 155$) and colorectal (colorect.) ($n = 216$) tumours. **m**, Mice ($n = 14$ per group) were subjected to azoxymethane plus dextran sodium sulfate treatment for 68 days. Mice were treated with normal drinking water or with 20% mannose in drinking water until the clinical end point. Tumours were counted in the colon of each mouse. **n**, $Villin^{creER}Apc^{fl/+}Kras^{G12D/+}$ mice were aged until the clinical end point. Mice were treated with normal drinking water or with 20% mannose in drinking water from four days post-induction until the clinical end point ($n = 9$ mice (−mannose), $n = 8$ mice (+mannose)). Tumours were counted in the colon of each mouse. $n = 3$ independent experiments (**b**, **c**, **e**, **f**); $n = 5$ independent experiments (**d**). Data represent one independent experiment performed in technical triplicate (**g**) or are representative of two independent experiments (**a**). Data are mean ± s.e.m. and are analysed by a one-sided Mann–Whitney *U*-test. $^{***}P < 0.001$. Data were analysed by two-way ANOVA with Bonferroni correction (**c**, **e**), multiple two-sided unpaired *t*-test with Holm–Sidak correction (**d**), two-way ANOVA with Tukey correction (**h**–**k**), one-way ANOVA with Bonferroni correction (**l**), unpaired two-tailed Student's *t*-test (**m**) and one-sided Mann–Whitney *U*-test (**n**). $^{*}P < 0.05$, $^{**}P < 0.01$, $^{***}P < 0.001$, $^{****}P < 0.0001$.

(Extended Data Fig. 10a–f). Mannose does not invoke an endoplasmic-reticulum stress response, but affects transcription, translation and autophagy, although these effects were reversed by overexpression of *MPI*, which indicates that they are downstream of glucose metabolism (Extended Data Fig. 10g–l). Moreover, the ablation of autophagy did not affect mannose sensitivity, showing that autophagy inhibition is not the mechanism underlying the effects of the sugar (Extended Data Fig. 10m, n). In summary, we conclude that mannose represents a well-tolerated means to interfere with glucose metabolism that could potentially be used clinically, either alone or in combination with other forms of cancer therapy.

Online content

Any methods, additional references, Nature Research reporting summaries, source data, statements of data availability and associated accession codes are available at https://doi.org/10.1038/s41586-018-0729-3.

Received: 12 October 2017; Accepted: 5 October 2018;
Published online: 21 November 2018

1. Hanahan, D. & Weinberg, R. A. Hallmarks of cancer: the next generation. *Cell* **144**, 646–674 (2011).
2. Pavlova, N. N. & Thompson, C. B. The emerging hallmarks of cancer metabolism. *Cell Metab.* **23**, 27–47 (2016).
3. Thorens, B. & Mueckler, M. Glucose transporters in the 21st century. *Am. J. Physiol. Endocrinol. Metab.* **298**, E141–E145 (2010).
4. Cairns, R. A., Harris, I. S. & Mak, T. W. Regulation of cancer cell metabolism. *Nat. Rev. Cancer* **11**, 85–95 (2011).
5. Chaube, B. & Bhat, M. K. AMPK, a key regulator of metabolic/energy homeostasis and mitochondrial biogenesis in cancer cells. *Cell Death Dis.* **7**, e2044 (2016).
6. Zhang, C. S. et al. Fructose-1,6-bisphosphate and aldolase mediate glucose sensing by AMPK. *Nature* **548**, 112–116 (2017).
7. DeRossi, C. et al. Ablation of mouse phosphomannose isomerase (*Mpi*) causes mannose 6-phosphate accumulation, toxicity, and embryonic lethality. *J. Biol. Chem.* **281**, 5916–5927 (2006).
8. Fischer, U., Jänicke, R. U. & Schulze-Osthoff, K. Many cuts to ruin: a comprehensive update of caspase substrates. *Cell Death Differ.* **10**, 76–100 (2003).
9. Elmore, S. Apoptosis: a review of programmed cell death. *Toxicol. Pathol.* **35**, 495–516 (2007).
10. Westphal, D., Dewson, G., Czabotar, P. E. & Kluck, R. M. Molecular biology of Bax and Bak activation and action. *Biochim. Biophys. Acta* **1813**, 521–531 (2011).

11. Tait, S. W. & Green, D. R. Mitochondria and cell death: outer membrane permeabilization and beyond. *Nat. Rev. Mol. Cell Biol.* **11**, 621–632 (2010).
12. Pradelli, L. A. et al. Glycolysis inhibition sensitizes tumor cells to death receptors-induced apoptosis by AMP kinase activation leading to Mcl-1 block in translation. *Oncogene* **29**, 1641–1652 (2010).
13. Alves, N. L. et al. The Noxa/Mcl-1 axis regulates susceptibility to apoptosis under glucose limitation in dividing T cells. *Immunity* **24**, 703–716 (2006).
14. Coloff, J. L. et al. Akt-dependent glucose metabolism promotes Mcl-1 synthesis to maintain cell survival and resistance to Bcl-2 inhibition. *Cancer Res.* **71**, 5204–5213 (2011).
15. Quirce, R. et al. New insight of functional molecular imaging into the atheroma biology: ^{18}F-NaF and ^{18}F-FDG in symptomatic and asymptomatic carotid plaques after recent CVA. Preliminary results. *Clin. Physiol. Funct. Imaging* **36**, 499–503 (2016).
16. Sharma, V., Ichikawa, M. & Freeze, H. H. Mannose metabolism: more than meets the eye. *Biochem. Biophys. Res. Commun.* **453**, 220–228 (2014).
17. Chattopadhyay, U. & Bhattacharyya, S. Inhibition by monosaccharides of tumor associated macrophages mediated antibody dependent cell cytotoxicity to autologous tumor cells. *Neoplasma* **34**, 295–303 (1987).
18. Gartner, S. L. & Williams, T. J. Modulation of interleukin-1 induced thymocyte proliferation by D-mannose. *Thymus* **19**, 117–126 (1992).
19. Alton, G. et al. Direct utilization of mannose for mammalian glycoprotein biosynthesis. *Glycobiology* **8**, 285–295 (1998).
20. De Robertis, M. et al. The AOM/DSS murine model for the study of colon carcinogenesis: from pathways to diagnosis and therapy studies. *J. Carcinog.* **10**, 9 (2011).

Acknowledgements We thank J. Knight, D. Lewis and E. Johnson for help and advice. This work was supported by Worldwide Cancer Research (16-1194) and Cancer Research UK (A15816 and A17196).

Reviewer information *Nature* thanks H. Christofk, J. Cleveland and A. Villunger for their contribution to the peer review of this work.

Author contributions K.M.R., P.S.G. and A.D.B. conceived the study. P.S.G., J.O., J.-i.S., F.B., E.K. and S.R. conducted and analysed cell growth, cell death and enzyme assays and western blotting. P.S.G., S.C. and G. Mackay conducted and analysed metabolic experiments. V.J.A.B., D.M.G. and B.Z. performed animal experiments. G. Malviya and A.M. performed and analysed PET and MRI scans. C.N. performed immunohistochemistry. A.R., D.E., A.H. and D.M. generated and analysed tissue microarrays. P.S.G. and K.M.R. wrote the manuscript. I.A.M., O.J.S., J.E. and K.M.R. supervised the study.

Competing interests The authors declare no competing interests.

Additional information
Extended data is available for this paper at https://doi.org/10.1038/s41586-018-0729-3.
Supplementary information is available for this paper at https://doi.org/10.1038/s41586-018-0729-3.
Reprints and permissions information is available at http://www.nature.com/reprints.
Correspondence and requests for materials should be addressed to K.M.R.
Publisher's note: Springer Nature remains neutral with regard to jurisdictional claims in published maps and institutional affiliations.

METHODS

Cell culture, transfections and infections. All cell lines were from Beatson Institute stocks and were originally obtained from American Type Culture Collection or European Collection of Authenticated Cell Cultures repositories, apart from PATU-8902 (DMSZ, ACC-179) and KP-4 (RIKEN, RCB1005). A549, IGROV-1, Saos-2, U2OS, U2OS-E1a, SKOV-3, RKO and PATU-8902 cells were grown in DMEM high glucose supplemented with 10% FBS, glutamine (0.292 mg ml^{-1}) and penicillin (100 units per ml)–streptomycin (100 μg ml^{-1}) (all from Life Technologies). U2OS-E1a cells were generated in our laboratory and have been previously described[21]. K562 cells were grown in RPMI-1640 and KP-4 cells were grown in IMDM (Life Technologies) with 20% FBS, supplemented with penicillin (100 units per ml)–streptomycin (100 μg ml^{-1}). The B16-F1 mouse skin melanoma cell line was a gift from L. Machesky (Cancer Research UK Beatson Institute) and cells were maintained in DMEM (Thermo Fisher Scientific, 21969035) supplemented with 10% FBS (Thermo Fisher Scientific, 10270106), 2 mM L-glutamine (Thermo Fisher Scientific, 25030032), and penicillin–streptomycin (Thermo Fisher Scientific, 15140122). LLC mouse Lewis lung carcinoma cells were a gift from S. Zanivan (Cancer Research UK Beatson Institute) and were maintained in RPMI-1640 (Thermo Fisher Scientific, 31870074), 10% FBS, 10 mM HEPES (Thermo Fisher Scientific, 15630080), 2 mM L-glutamine and penicillin–streptomycin. These cell lines were confirmed to be free of mycoplasma.

Cells were transfected using calcium phosphate precipitates as previously described[16]. U2OS-E1a cells were infected with virus containing pBabe-puro-empty or pBabe-puro-Bcl-X_L following the same protocol as previously published[21]. U2OS-E1a cells were infected with virus containing pLZRS empty or pLZRS HA-Mcl-1 (provided by S. Tait)[22]. U2OS-E1a-infected cells were selected in DMEM 10% FBS containing 600 μg ml^{-1} of neomycin for 2 weeks. U2OS control and Bax/Bak CRISPR cells were provided by S. Tait.

The following siRNAs were used: PMI siRNA-1 (Dharmacon, J-011729-05-0002), PMI siRNA-2 (Dharmacon, J-011729-06-0002), PMI siRNA-3 (Dharmacon, J-011729-07-0002), PMI siRNA-4 (Dharmacon, J-011729-08-0002), NTC1 (Dharmacon, D-001810-03-20) and NTC2 (Dharmacon, D-001810-04-20).

lentiCRISPR v2 was a gift from F. Zhang (Addgene plasmid 52961)[23]. The following single-guide RNA sequences were used in the experiments. NTC 1: GTAGCGAACGTGTCCGGCGT; NTC 2: GCTTGAGCACATACGCGAAT; ATG5: AAGAGTAAGTTATTTGACGT; ATG7: GAAGCTGAACGAGTATCGGC; Casp8: GCCTGGACTACATTCCGCAA; FADD: TTCCTATGCCT CGGGC GCGT; BAX: AGTAGAAAAGGGCGACAACC; BAK: GCCATGCTGGTAGAC GTGTA; NOXA: TCGAGTGTGCTACTCAACTC.

The following shRNAs were used: pGIPZ-non-targeting control (NTC) (Dharmacon, RHS4346), PMI 1 (Dharmacon, RMM4431-200352145, Clone ID: V2LMM_110673) and PMI 2 (Dharmacon, RMM4431-200355616, Clone ID: V2LMM_203337).

pLX304 was a gift from D. Root (Addgene plasmid 25890). Human PMI cDNA was amplified using pCMV-Sport-MPI (Dharmacon, MHS6278-202802339) as a template and inserted into pDONR221 vector (Thermo Fisher Scientific, 12536017) using Gateway BP Clonase II Enzyme mix (Thermo Fisher Scientific, 11789020). PMI cDNA was then transferred into a pLX304 destination vector using Gateway LR Clonase II Enzyme mix (Thermo Fisher Scientific, 11791020). Lentivirus production and infection were carried out as described previously[24].

Cell culture treatments. *Mannose treatment.* Cells were seeded in six-well plates and incubated overnight at 37 °C. The following day, the medium was replenished with fresh full growth medium (DMEM, RPMI-1640 or IMDM) containing 25 mM D-mannose (DMEM or IMDM) or 11.11 mM D-mannose (RPMI-1640). Other sugars were added to a concentration of 25 mM: D-glucose (Sigma-Aldrich, G8270), D-fructose (Sigma-Aldrich, F3510), D-galactose (Sigma-Aldrich, G5388), L-fucose (Sigma-Aldrich, F2252 and Cayman Chemical, 16479). New stocks were prepared every two weeks of 1 M mannose in Milli-Q water and sterilized by filtering through a 0.22-μm pore filter. For control conditions, the same volume of Milli-Q water was added to the medium. Cells were left for at least 24 h for cell-death experiments or for 6 h for metabolic experiments. Cell death was blocked by treatment with zVAD-FMK (Apax Labs, A1902). Where indicated, cells were also treated with 2-deoxy-D-glucose (Sigma-Aldrich, D8375), tunicamycin (Sigma-Aldrich, T7765) or chloroquine (Sigma-Aldrich, C6628).

^{13}C-labelled sugars. The day after seeding, cells were washed three times with abundant PBS before adding glucose-free DMEM (supplemented with 10% dialysed FBS, 2 mM glutamine, 100 units per ml of penicillin and 100 μg ml^{-1} of streptomycin). Depending on the experiments, this medium could contain 5 mM of 1,2-$^{13}C_2$-glucose alone, together with $^{13}C_6$-mannose or 5 mM $^{13}C_6$-mannose alone. Stocks of 1,2-$^{13}C_2$-glucose and $^{13}C_6$-mannose were prepared at a concentration of 0.5 M in Milli-Q water before sterilization by filtering through a 0.22-μm pore filter.

Chemotherapeutic drugs. Cells were plated overnight and then incubated for the indicated times in control or mannose-containing medium. After one day of incubation, fresh control and mannose-containing media were prepared and drugs were added as described for each experiment. The drugs used were cisplatin (Sigma-Aldrich, C2210000) and doxorubicin (Sigma-Aldrich, D1515).

RT–qPCR. RT–qPCR was carried out as previously described[24] using primers for MCL1 (Qiagen, QT 00094122) and BCL2L1 (Qiagen, QT00997423). mRNA levels were determined by the relative standard curve method, normalized to 18S.

Western blotting. Protein extraction was performed as previously described[25]. Protein lysates were separated by SDS–PAGE and blotted onto nitrocellulose membranes. Western blot analysis was performed according to standard techniques as previously described[25]. The following antibodies were used at a dilution of 1:1,000 unless otherwise stated: anti-β-actin (Abcam, ab8227), anti-Mcl-1 (Cell Signaling, 4572), anti-ERK2 (Santa Cruz, sc-154), anti-Bcl-X_L (Cell Signaling, 2762), anti-HSP-90β (Santa Cruz, sc-1057), anti-PARP (Cell Signaling, 9542), anti-cleaved caspase-3 (Cell Signaling, 9664), anti-FADD (BD Transduction Laboratories, F36620), anti-caspase-8 (Cell Signaling, 4790), anti-Bax (BD Transduction Laboratories, 610983), anti-Bak (Cell Signaling, 6947), anti-Bim (Cell Signaling, 2993), anti-Noxa (Novus Biologicals, NB-600-1159), anti-phospho-AMPKα (Cell Signaling, 2535), anti-AMPKα (Cell Signaling, 5832), anti-PMI (Abcam, 128115), anti-LC3B (Cell Signaling, 2775S, 1:1,500), anti-β-actin (Cell Signaling, 4670S, 1:2,000), anti-ATG5 (Cell Signaling, 12994S), anti-ATG7 (Cell Signaling, 8558S), anti-Bip (also known as GRP78; Cell Signaling, 3177S) and anti-p62 (BD Biosciences, 610833, 1:2,000). Mouse PMI protein was detected using rabbit polyclonal PMI antibody (Proteintech, 14234-1-AP). Validation was based on information provided in the manufacturers' datasheets. In addition, as indicated in the manuscript, we used RNAi or CRISPR–Cas9 to validate the antibodies used to detect the following proteins: Bax, Bak, caspase-8, FADD, PMI, Atg5 and Atg7.

Metabolic extraction of intracellular metabolites. Cells were seeded at a concentration of 100,000 cells per well in six-well plates. The next morning, the medium was replenished with fresh full medium and cells were kept under these conditions for another 24 h to stabilize their metabolism. Approximately 36–40 h after being plated, cells were treated under different conditions as described, using full growth medium or glucose-free medium in the presence or absence of unlabelled sugars or labelled sugars for 6 h. After a 6-h incubation at 37 °C, intracellular metabolites were extracted.

The medium was aspirated and six-well plates were placed on ice and washed thoroughly with 4 °C PBS three times before the addition of 500 μl extraction solvent (50% methanol, 30% acetonitrile, 20% Milli-Q water) to each well. Plates were then agitated at 4 °C for 5 min to successfully extract intracellular metabolites and then centrifuged at 16,100*g* for 10 min at 4 °C. Supernatants were transferred into HPLC vials and stored at −80 °C before LC–MS analysis.

An Exactive Orbitrap mass spectrometer (Thermo Scientific) was used together with a Thermo Scientific Accela HPLC system. The HPLC setup consisted of a ZIC-pHILIC column (SeQuant, 150 mm × 2.1 mm, 5 μm, Merck KGaA) with a ZIC-pHILIC guard column (SeQuant, 20 mm × 2.1 mm) and an initial mobile phase of 20% 20 mM ammonium carbonate, pH 9.4 and 80% acetonitrile. Cell extracts (5 μl) were injected and metabolites were separated over a 15-min mobile phase gradient, decreasing the acetonitrile content to 20%, at a flow rate of 200 μl min^{-1} and a column temperature of 45 °C. The total analysis time was 23 min. For longer runs of 37 min, a 30-min gradient with the same solvents was used, at a flow rate of 100 μl min^{-1} and a column temperature of 30 °C[26]. All metabolites were detected across a mass range of 75–1,000 *m*/*z* using the Exactive mass spectrometer at a resolution of 25,000 (at 200 *m*/*z*), with electrospray ionization and polarity switching to enable both positive and negative ions to be determined in the same run. Lock masses were used and the mass accuracy obtained for all metabolites was below 5 p.p.m. Data were acquired with Thermo Xcalibur software (version 2.2).

The peak areas of different metabolites were determined using Thermo TraceFinder software (version 3.2), in which metabolites were identified by the exact mass of the singly charged ion and by known retention time on the HPLC column. Commercial standards of all metabolites detected had been analysed previously on this LC–MS system with the pHILIC column. The ^{13}C labelling patterns were determined by measuring peak areas for the accurate mass of each isotopologue of many metabolites. Intracellular metabolites were normalized to the protein content of the cells, measured at the end of the experiment by the Lowry assay[27]. As the proteins precipitate upon addition of the metabolite extraction solvent, protein content was measured in the wells after the metabolites were extracted.

Translation assay. Cells at 50% confluency were pretreated with or without 25 mM mannose for 24 h or with 100 μg ml^{-1} cycloheximide for 1 h. [^{35}S]methionine (1 MBq) (Perkin Elmer, EasyTag EXPRESS^{35}S Protein Labelling Mix, NEG772002MC) was added to the culture medium (2 ml per well in a six-well plate) for 30 min. Cells were washed in ice-cold PBS, then lysed in lysis buffer (10 mM Tris pH 7.5, 50 mM NaCl, 0.5% NP40, 0.5% SDS, benzonase (Sigma-Aldrich E1014, 2 μl per 10 ml of lysis buffer)). Proteins were precipitated in 25% trichloroacetic acid at 4 °C for 30 min. The precipitates were washed on glass-fibre filters (Whatman 934-AH, 1287-024) with 70% ethanol followed by acetone, dried, and

incorporation of ^{35}S was quantified in a liquid scintillation counter. The results were calculated as relative ^{35}S incorporation per 10^5 cells.

Transcription assay. Cells at 50% confluency were pretreated with 25 mM mannose or with a control for 24 h, or with 5 μM actinomycin D for 1 h. [^{32}P]UTP (1.1 MBq) (Perkin Elmer, BLU007H001MC) was added to the culture medium (2 ml per well in a six-well plate) for 6 h. Cells were washed in PBS and mRNA was prepared using the Dynabeads mRNA DIRECT Kit (Life Technologies, 61012). ^{32}P-labelled mRNA was quantified in a liquid scintillation counter and the results were calculated as relative [^{32}P]UTP incorporation per 10^5 cells.

PMI enzymatic assay. Cells were grown to confluence, washed with PBS and collected by centrifugation (5 min, 150*g* at 4 °C). Cell pellets were lysed by three freeze–thaw cycles. Post-nuclear protein fractions (40 μg) were used to determine PMI activities in each cell line tested by means of a coupled enzymatic reaction. In brief, samples were incubated in a buffer containing 200 mU of PGI (Roche, 10 127 396 001), 500 mM glucose-6-phosphate dehydrogenase, 1 mM $NADP^+$, 40 mM Tris-HCl pH 7.4, 6 mM $MgCl_2$, 5 mM Na_2HPO_4/KH_2PO_4. Reactions were initiated by the addition of 1 mM mannose-6-phosphate, and the production of $NADPH/H^+$ was assessed for 2 h at room temperature by measuring the optical density at 340 nm (OD_{340nm}). In parallel, western blots directed against PMI and ERK2 were performed to examine the correlation between PMI activities and PMI expression levels in each cell line analysed.

Proteasome assay. Cells were seeded 24 h before 24-h treatments using media either with or without mannose supplementation (25 mM). A luminescence-based assay (Proteasome-Glo chymotrypsin-like cell-based assays, Promega) was performed according to the manufacturer's protocol. The measured proteasome activities were normalized to cell number by counting cells at the end of each experiment. Cells were treated with 10 μM MG132 as a control for the specificity of the assay.

Lowry assay. The Lowry assay was used to determine the total protein content for each one of the triplicates from the metabolic experiments. First, 500 μl of solution A (70% Milli-Q water, 20% 5 M NaOH, 10% 2,5-dimethoxy-4-chloroamphetamine) was added to each well from a six-well plate and left under agitation for 20 min. Next, 5 ml of solution B (0.5 g NaCu-EDTA, 40 g Na_2CO_3, 8 g NaOH in 2 l) was added to each well and left for 40 min. Then, 500 μl of Folin reagent was added to each well and left for a minimum of 15 min until a blue colour was observed in each well. One or two six-well plates were used to construct a standard curve of protein concentration with BSA. Finally, 200 μl from each well was separately transferred to a 96-well plate and the absorbance was measured at 750 nm. The protein concentration was then measured by calculating the equation of the standard curve and extrapolating the absorbance of each well.

Flow cytometry. Flow cytometry for unfixed cells (cell-death assay) was conducted as previously described[28], and a FACSCalibur or ATTune NXT flow cytometer was used for the analysis.

Animal experiments. All in vivo xenograft experiments were performed using six-week old female CD1-nude mice or C57/BL6J wild-type mice as approved by the Glasgow University Animal Welfare and Ethical Review Body and in accordance with UK Home Office guidelines. Mice were placed five per cage with free access to water and food (chow diet). Experimental cohort sizes were based on previous similar studies that have given statistical results while also respecting the limited use of animals in line with the 3R system: replacement, reduction, refinement. In no cases were mice maintained once the tumour size limit that was permitted in our Home Office license (15 mm in any direction) had been reached. All treatment studies were randomized, but did not involve blinding.

KP-4 cells (5×10^6 cells) were injected subcutaneously with 100 μl of Matrigel in either the right flank or both the left and the right flanks. LLC cells (1×10^6 cells) and B16-F1 cells (1×10^6 cells) were injected subcutaneously in 200 μl or 100 μl of PBS suspension, respectively. Mice were weighed and tumours were measured using callipers three times per week (usually on Monday, Wednesday and Friday of each week). The calculation of tumour volume was as follows: $(L \times S^2)/2$ (where L is the longest length and S is the shortest length).

For mannose treatment, normal drinking water was exchanged for 200 ml of 20% mannose in drinking water (w/v) and it was replaced once every week. Mice received mannose by oral gavage (200 μl) three times per week from the same stock of 20% mannose in water.

For doxorubicin treatments, each mouse received intraperitoneal injections at a concentration of 5 mg kg^{-1} once per week. Stocks of 1 mg ml^{-1} doxorubicin (Sigma-Aldrich, D1515) were prepared in Milli-Q water.

For azoxymethane (AOM) + dextran sodium sulfate (DSS) experiments, mice were injected with a single dose of AOM (Sigma-Aldrich, A5486) at 10 mg kg^{-1}. Five days after AOM injection, mice received three cycles of 1.5% DSS (MP Biomedical, 0216011080) in water; each cycle lasted five consecutive days, with one week in between each cycle. In the week between each cycle, mice received normal water or 20% (w/v) mannose water. After the last cycle of DSS, mice were maintained with normal water or mannose for two weeks before being killed on day 68.

Tissue collection. All mice were killed by CO_2-mediated euthanasia[29] before collecting any tissue sample. Mice were placed in a cage and exposed to CO_2 for 100 s before neck dislocation.

Xenografted tumours were removed and detached from the skin and cut in half. One half of each tumour was fixed for 24–30 h in 10% neutral buffered formalin at room temperature. Formalin was then exchanged for 70% ethanol before histology.

The colons of mice from AOM + DSS carcinogenesis experiments were collected and fixed in formalin for histological processing.

For the experiments with the genetically engineered mouse model, $Villin^{creER}Apc^{fl/+}Kras^{G12D/+}$ mice[30] aged 6–12 weeks were given a single intraperitoneal injection of 80 mg kg^{-1} tamoxifen (Sigma-Aldrich, T5648). Four days post-induction, drinking water was exchanged for fresh drinking water or 20% mannose in drinking water (w/v) and given freely, this was replaced every week. Mice were aged until the clinical end point—when they displayed anaemia, hunching or weight loss. Colons were pinned out into 10% neutral buffered formalin and the number of tumours was counted.

Blood sampling and blood metabolic extraction. To measure blood mannose levels, tail tipping was performed. Blood samples were directly frozen using dry ice and stored at −80 °C until metabolic extraction was performed.

For metabolic extraction of whole blood, 2–5 μl of each sample was diluted in 100–250 μl of metabolic extraction buffer on ice for 5 min (1:50 dilution). Then, all samples were centrifuged at 17,949*g* at 4 °C for 15 min. Finally, 100 μl of the supernatant from each sample was transferred into HPLC vials and stored at −80 °C until LC–MS analysis.

PET and MRI scanning. Mice with KP-4 cells xenografts ($n = 9$, weight 24.6 ± 1.8 g) received either 200 μl of 20% w/v mannose in water (treatment group) or normal water (control group) by oral gavage 20 min before the injection of [^{18}F]FDG. [^{18}F]FDG (12.9 ± 1MBq) in 200 μl of normal saline was administered via an intravenous bolus injection in the tail vein. After an uptake phase of 30 min, PET and MRI scans were sequentially performed using a nanoScan (Mediso Ltd) PET/MRI (1T) scanner. Mice were maintained under 2–2.5% isoflurane in medical air during the injection and imaging procedures. Static PET acquisitions were performed for 15 min, and subsequently whole body T1 GRE 3D Multi-FOV MRI scans (slice thickness 0.50 mm, repetition time (TR) 10 ms, echo time (TE) 2.3 ms, flip angle 12°) were performed to obtain anatomical references. For quantitative assessments of scans, regions of interest (ROI) were manually drawn around the edge of the tumour xenograft on MRI scans by visual inspection using PMOD software version 3.504 (PMOD Technologies) and the same ROI was copied on the respective PET scans. Tumour ROIs were slightly different between scans depending on the positions and angles of the mice on the scanner, therefore separate ROIs for each scan were drawn. The percentage injected dose per ml (%ID ml^{-1}) was calculated using the formula %ID ml^{-1} = ROI activity (kBq ml^{-1}) / injected dose × 100%. Data were reported as average %ID $ml^{-1} \pm$ s.d. Student's *t*-tests were used when comparing data between mannose-treated and control mice.

Tissue microarray PMI staining. Tissue microarrays (TMAs) were first placed in xylene for 5 min before three washes of 1 min each (two in ethanol and one in 70% ethanol). TMAs were washed for 5 min in deionized water and then held for 25 min at 98 °C in a PT module using pH 6 sodium citrate retrieval buffer. They were further washed once in tris-buffered Tween (TbT) before blocking endogenous peroxidase for 5 min. TMAs were washed again using TbT and stained with PMI antibody (1C7, 1:50 dilution) for 1 h. TMAs were washed in TbT before and after incubation for 30 min in a mouse EnVision detection system. A 10-min incubation in 3,3′-diaminobenzidine tetrahydrochloride was then perfomed. TMAs were again washed with deionized water (1 min) before and after incubation with haematoxylin Z, followed by post-incubation with 1% acid alcohol. This was followed by a 30-s wash with deionized water, and then incubation with Scott's Tap Water substitute (1 min) and deionized water (1 min).

BrdU staining. Xenografted tumours were embedded in paraffin, after which sections of an appropriate thickness were cut and kept at 60 °C overnight. Sections were first placed in xylene for 5 min before three washes of 1 min each (two in ethanol and one in 70% ethanol). Sections were washed for 5 min in deionized water and then held for 25 min at 98 °C in a PT module using pH 6 sodium citrate retrieval buffer. They were further washed once in TbT before blocking endogenous peroxidase for 5 min. Sections were washed in TbT before and after incubation with BrdU antibody (BD Biosciences 347580, 1:200 dilution) for 35 min. Sections were washed in TbT before and after incubation for 30 min in a mouse EnVision detection system. A 10-min incubation in 3,3′-diaminobenzidine tetrahydrochloride was then perfomed. Sections were again washed with deionized water (1 min) before and after incubation with haematoxylin Z, followed by post-incubation with 1% acid alcohol. This was followed by a 30-s wash with deionized water, and then incubation with Scott's Tap Water substitute (1 min) and deionized water (1 min).

Tissue microarrays. TMAs from ovarian, breast, colorectal, prostate and renal cancer were stained for PMI. The microarrays were scanned using a digital slide scanner (SCN 400 F, Leica Biosystems) and were scored for PMI expression on the basis of the percentage of tumour that showed negative, low, medium or high expression. Each sample was scored with a number between 0 and 300 according to the following equation: Score = (0 × negative) + (1 × low) + (2 × medium) + (3 × high).

Statistical analysis and reproducibility. All presented data were analysed using GraphPad Prism software. Four different statistical analyses were performed depending on the data from the different experiments shown, typically one-way ANOVA, two-way ANOVA, log-rank (Mantel–Cox) test and Student's *t*-tests that could be paired or unpaired and one-tailed or two-tailed. Four levels of significance were determined: $*P < 0.05$, $**P < 0.01$, $***P < 0.001$, $****P < 0.0001$, with NS indicating no significance. Where a representative experiment is shown, the number of times the same result was observed in independent experiments is detailed in the corresponding figure legend.

Reporting summary. Further information on research design is available in the Nature Research Reporting Summary linked to this paper.

Data availability

The data supporting the findings of this study are available within the paper and its Supplementary Information. Source Data for Figs. 1–4 and Extended Data Figs. 1–10 are available with the online version of the paper. Data are available from the corresponding author upon reasonable request.

21. Long, J. S. et al. Extracellular adenosine sensing—a metabolic cell death priming mechanism downstream of p53. *Mol. Cell* **50**, 394–406 (2013).
22. Riley, J. S. et al. Mitochondrial inner membrane permeabilisation enables mtDNA release during apoptosis. *EMBO J.* **37**, e99238 (2018).
23. Sanjana, N. E., Shalem, O. & Zhang, F. Improved vectors and genome-wide libraries for CRISPR screening. *Nat. Methods* **11**, 783–784 (2014).
24. Sakamaki, J. I. et al. Bromodomain protein BRD4 is a transcriptional repressor of autophagy and lysosomal function. *Mol. Cell* **66**, 517–532 (2017).
25. Mrschtik, M. et al. DRAM-3 modulates autophagy and promotes cell survival in the absence of glucose. *Cell Death Differ.* **22**, 1714–1726 (2015).
26. Mackay, G. M., Zeng, L., van den Broek, N. J. F. & Gottlieb, E. Analysis of cell metabolism using LC–MS and isotope tracers. *Methods Enzymol.* **561**, 171–196 (2015).
27. Karvela, M. et al. ATG7 regulates energy metabolism, differentiation and survival of Philadelphia-chromosome-positive cells. *Autophagy* **12**, 936–948 (2016).
28. Rosenfeldt, M. T. et al. E2F1 drives chemotherapeutic drug resistance via ABCG2. *Oncogene* **33**, 4164–4172 (2014).
29. Rosenfeldt, M. T. et al. p53 status determines the role of autophagy in pancreatic tumour development. *Nature* **504**, 296–300 (2013).
30. Cammareri, P. et al. TGFβ pathway limits dedifferentiation following WNT and MAPK pathway activation to suppress intestinal tumourigenesis. *Cell Death Differ.* **24**, 1681–1693 (2017).

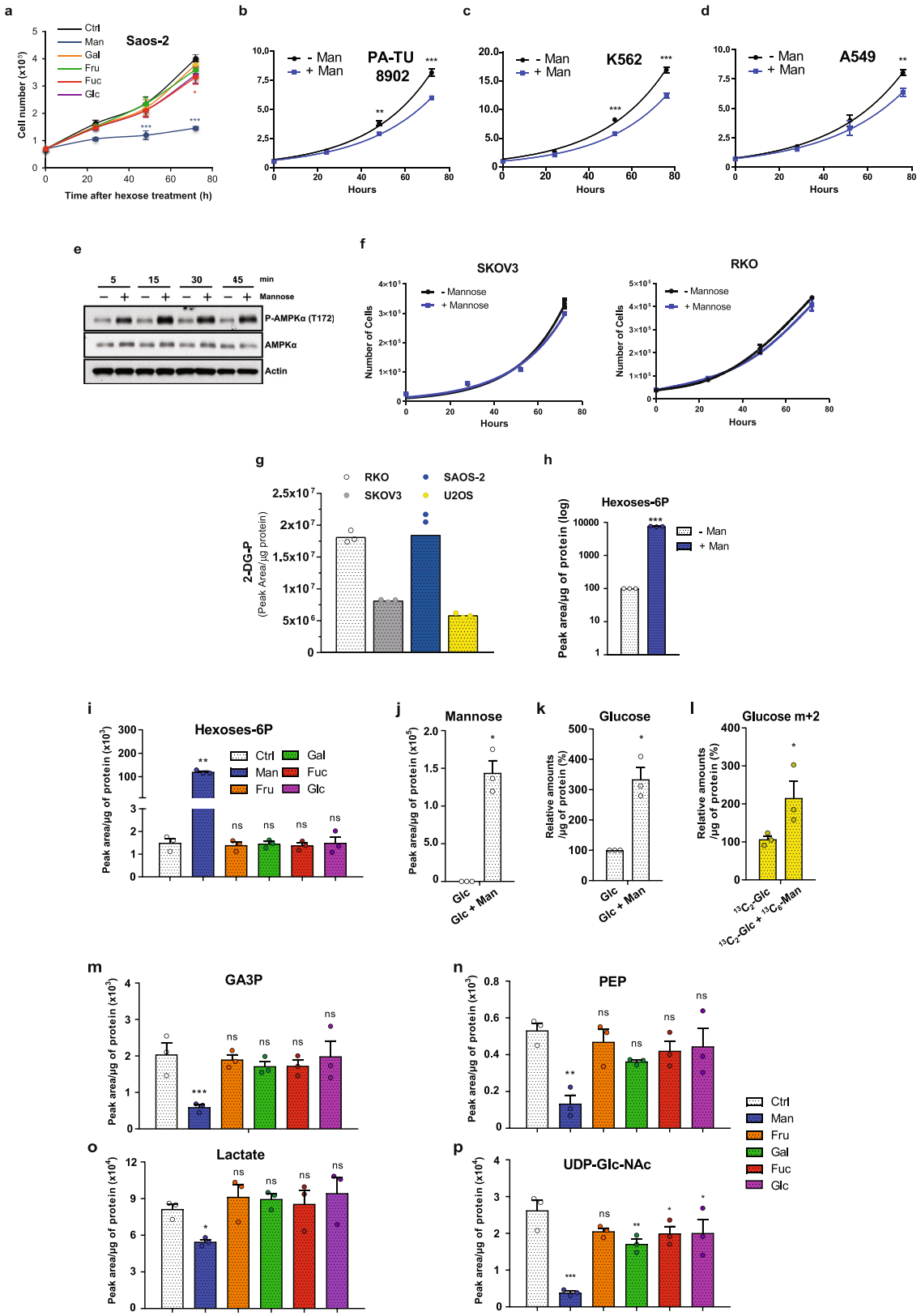

Extended Data Fig. 1 | See next page for caption.

Extended Data Fig. 1 | Mannose affects cell growth and metabolism. **a**, Growth curves of Saos-2 cells supplemented without (control) or with 25 mM of hexoses (man, mannose; gal, galactose; fru, fructose; fuc, fucose; glc, glucose). **b**–**d**, Growth curves of PA-TU-8902 (**b**) and A549 cells (**d**) in DMEM alone or with an additional 25 mM mannose; K562 cells in 10% FBS RPMI-1640 medium with or without 11.1 mM mannose (**c**). **e**, Western blots showing the levels of phospho-AMPKα (T172) and total AMPKα after 5, 15, 30 and 45-min incubation of U2OS-E1a with standard medium or medium supplemented with 25 mM mannose. **f**, Growth curves of SKOV3 and RKO cells in DMEM alone or with an additional 25 mM mannose. **g**, Levels (expressed as peak area per microgram of protein) of 2-deoxyglucose-phosphate (2-DG-P) in RKO, SKOV3, SAOS-2 and U2OS-E1a (U2OS) cells incubated with 10 mM 2-deoxyglucose for 6 h in the presence of 25 mM mannose in the culture medium (DMEM). Data are the average of three technical replicates and are representative of two independent experiments. **h**, Levels (measured as the percentage of peak area per microgram of protein, on a $\log_{10}$ scale) of hexoses-6-phosphate (hexoses-6P) in U2OS-E1a cells after 6 h incubation in 10% dialysed FBS with 5 mM glucose in DMEM either with or without 5 mM mannose. **i**, Peak area per microgram of protein of hexoses-6-phosphate in U2OS-E1a cells incubated for 6 h in DMEM, with or without an additional 25 mM of the indicated sugars. **j**, **k**, Peak area per microgram of protein of intracellular non-phosphorylated mannose (**j**) or relative amounts of glucose (**k**) after a 6 h incubation of U2OS-E1a cells in 5 mM glucose in DMEM, with or without 5 mM mannose. **l**, Relative amount per microgram of protein of non-phosphorylated glucose $m + 2$ after 6 h incubation of U2OS-E1a cells in glucose-free DMEM either with 5 mM 1,2-$^{13}C_2$-D-glucose alone or with 5 mM 1,2-$^{13}C_2$-D-glucose and 5 mM $^{13}C_6$-D-mannose. **m**–**p**, Peak area per microgram of protein of glyceraldehyde-3-phosphate (GA3P) (**m**), phosphoenolpyruvate (PEP) (**n**), lactate (**o**) and UDP-GlcNAc (**p**) in U2OS-E1a cells after 6 h incubation in DMEM, with or without an additional 25 mM of the indicated sugars. $n = 3$ independent experiments (**a**–**d**, **f**, **h**–**p**). Data are representative of two independent experiments (**e**). All data are mean ± s.e.m. and were analysed by one-way ANOVA (**i**, **m**–**p**), two-way ANOVA followed by Tukey's multiple comparisons (**a**) or paired two-tailed Student's *t*-test (**h**, **j**–**l**). $*P < 0.05$, $**P < 0.01$, $***P < 0.001$.

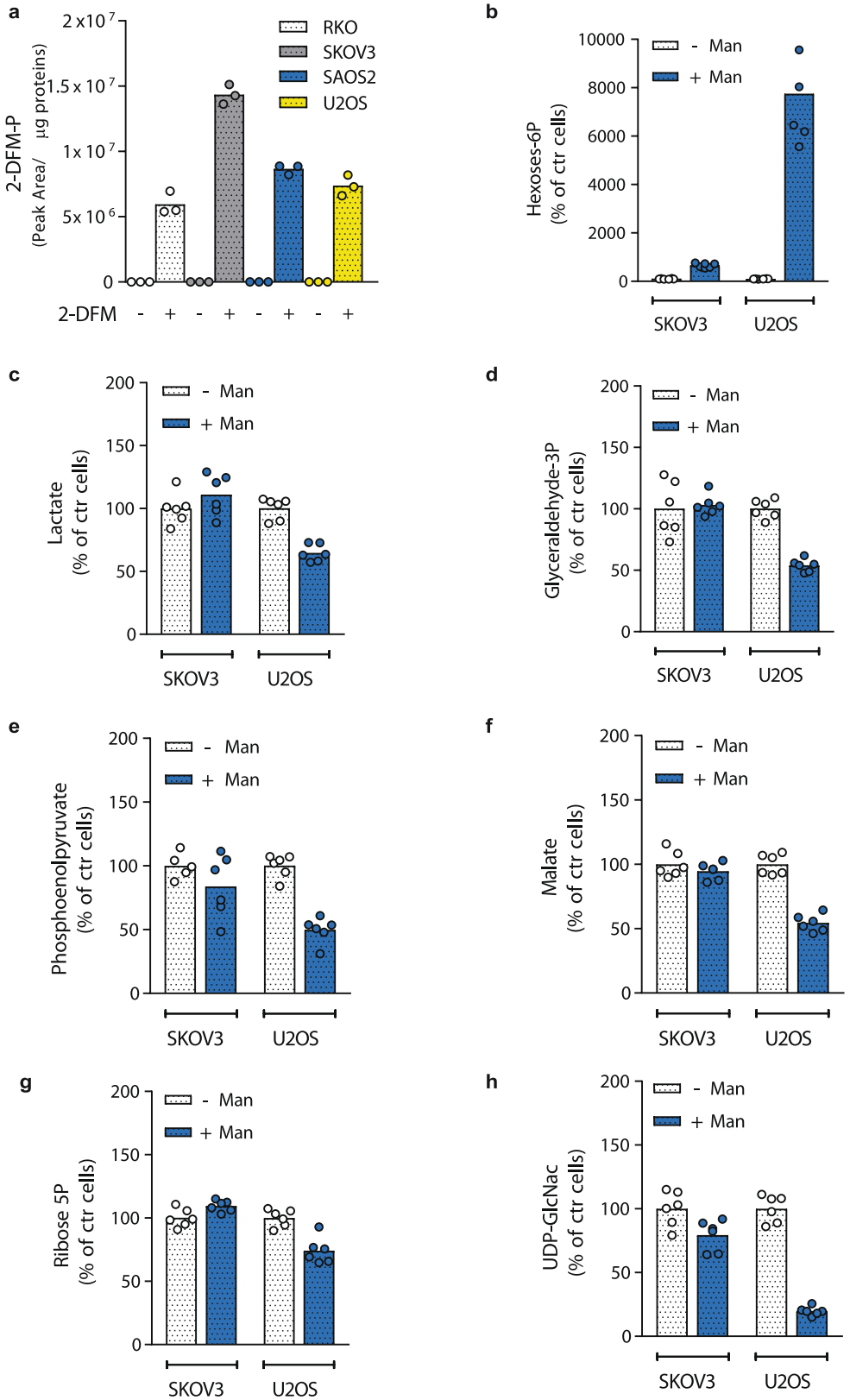

Extended Data Fig. 2 | Mannose sensitivity is not associated with mannose uptake but with changes in cellular metabolism. a, Levels (expressed as peak area per microgram of proteins) of 2-deoxy-2-fluoro-D-mannose-phosphate (2-DFM-P) in RKO, SKOV3, SAOS-2 and U2OS-E1a (U2OS) cells after 6 h treatment with or without 2 mM 2-deoxy-2 fluoro-D-mannose. **b**–**h**, Relative levels of hexoses-6-phosphate (**b**), lactate (**c**), glyceraldehyde-3-phosphate (glyceraldehyde-3P) (**d**), phosphoenolpyruvate (**e**), malate (**f**), ribose-5-phosphate (ribose-5P) (**g**) and UDP-GlcNac (**h**) in SKOV3 and U2OS-E1a (U2OS) cells after 6 h treatment with or without 25 mM mannose in the culture medium (DMEM). Data in **a** are the average of three technical replicates and are representative of two independent experiments. In **b**–**h**, $n = 2$ independent experiments, each involving technical triplicates. All data are mean.

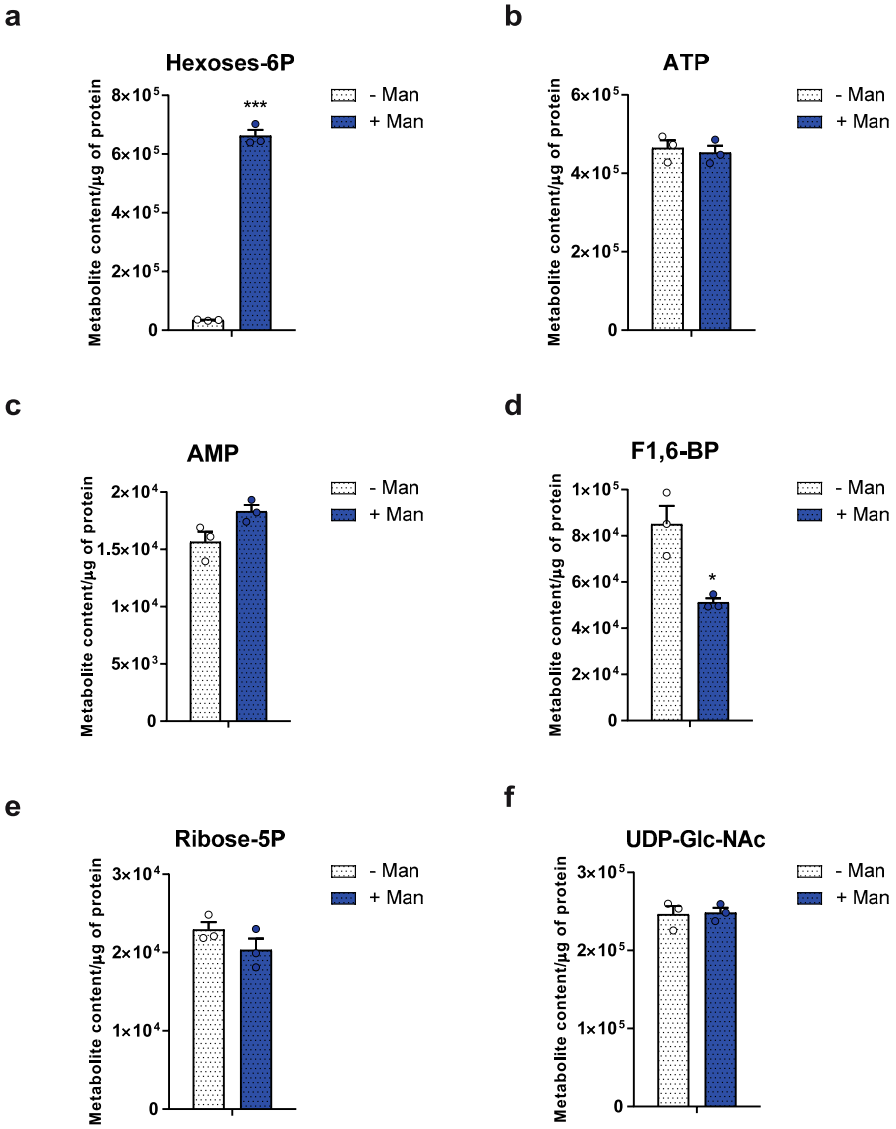

Extended Data Fig. 3 | Mannose has a rapid effect on cellular metabolism. Metabolite content (expressed as peak area per microgram of proteins) of hexoses-6-phosphate (**a**), ATP (**b**), AMP (**c**), fructose-1, 6-bisphosphate (F1,6-BP) (**d**), ribose-5-phosphate (**e**) and UDP-GlcNac (**f**) in U2OS-E1a (U2OS) cells after 5 min treatment with or without 25 mM mannose in the culture medium (DMEM). $n = 3$ independent experiments, presented as mean ± s.e.m. and analysed by a two-tailed unpaired *t*-test. $^{*}P < 0.05$, $^{***}P < 0.001$.

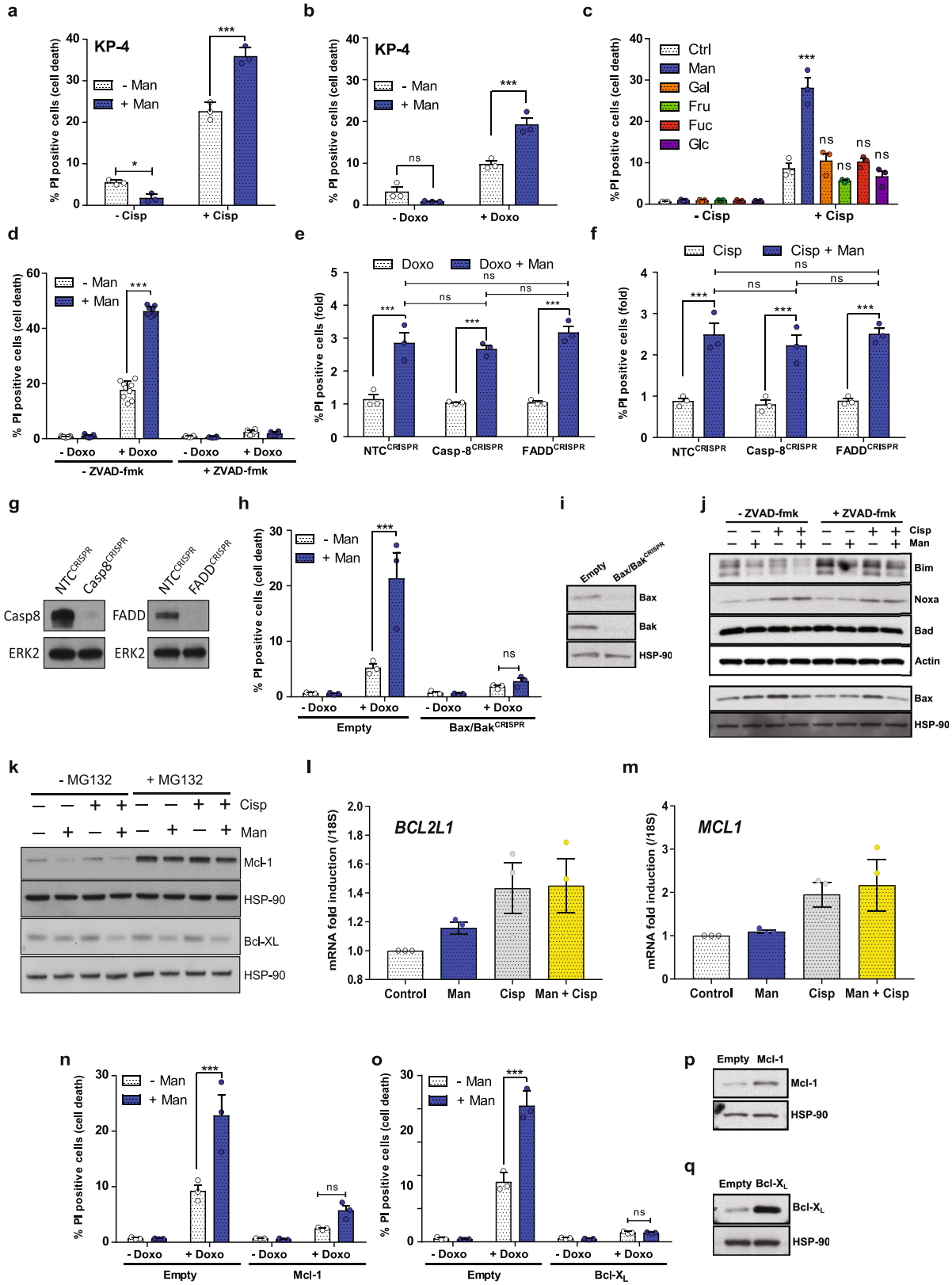

Extended Data Fig. 4 | See next page for caption.

Extended Data Fig. 4 | Mannose sensitizes cells to chemotherapy-induced cell death via the intrinsic apoptotic pathway. a, **b**, Percentage of propidium-iodide-positive KP-4 cells after 24 h treatment with 40 μM cisplatin (**a**) or 1 μg ml^{-1} doxorubicin (**b**) in the presence or absence of 25 mM mannose. **c**, Percentage of U2OS-E1a propidium-iodide-positive cells after 24 h treatment with or without 10 μM cisplatin in DMEM with or without 25 mM of the indicated additional sugars. **d**, Percentage of U2OS-E1a propidium-iodide-positive cells after 24 h treatment with or without 1 μg ml^{-1} doxorubicin, with or without 25 mM mannose and with or without 50 μM zVAD-FMK. **e**, **f**, Fold increase of the percentage of propidium-iodide-positive Saos-2 (NTC, caspase-8 and FADD CRISPR) cells upon 24 h treatment in DMEM with or without 1 μg ml^{-1} doxorubicin (**e**) or 10 μM cisplatin (**f**) and with or without 25 mM mannose. **g**, Western blots showing the levels of caspase-8, FADD and ERK2 in NTC, caspase-8 and FADD CRISPR Saos-2 cells. **h**, Percentage of empty and Bax/Bak CRISPR U2OS-E1a propidium-iodide-positive cells with or without 1 μg ml^{-1} doxorubicin and with or without 25 mM mannose. **i**, Western blots showing the levels of Bax, Bak and HSP90 in empty and Bax/Bak CRISPR U2OS-E1a cells. **j**, Western blots showing the levels of Bim, Noxa, Bad, Bax, Actin and HSP-90 in U2OS-E1a cells after 24 h treatment with or without 10 μM cisplatin, with or without 25 mM mannose and with or without 50 μM zVAD-FMK. The HSP-90 blot is identical to the one shown in Fig. 2f as the blots are from the same experiment. **k**, Western blots showing the levels of Mcl-1 and Bcl-X_L in U2OS-E1a cells after 48 h with or without 10 μM cisplatin, with or without 25 mM mannose and in the absence or presence of 10 μM MG132 as indicated. **l**, **m**, PCR with reverse transcription (RT–PCR) showing the levels of *BCL2L1* (Bcl-X_L) (**l**) and *MCL1* (**m**) mRNAs in U2OS-E1a cells after 48 h treatment with 10 μM cisplatin alone, 25 mM mannose alone, or both 10 μM cisplatin and 25 mM mannose, in the presence of 50 μM zVAD-FMK. **n**, **o**, Percentage of U2OS-E1a (empty), Mcl-1 and Bcl-X_L overexpressing propidium-iodide-positive cells after 24 h treatment with or without 1 μg ml^{-1} doxorubicin and with or without 25 mM mannose. **p**, **q**, Western blot showing the levels of Mcl-1, Bcl-X_L and HSP-90 in U2OS-E1a (empty), Mcl-1 and Bcl-X_L overexpressing cells. $n = 3$ independent experiments (**a**–**c**, **e**, **f**, **h**, **l**–**o**). Data are representative of two independent experiments (**g**, **j**, **k**) or one experiment (**i**, **p**, **q**). In **d**, $n = 3$ independent experiments (each involving technical triplicates) (−zVAD-FMK) and $n = 2$ independent experiments (each involving technical triplicates) (+zVAD-FMK). All data are mean ± s.e.m. and were analysed by two-way ANOVA with Bonferroni correction (**a**–**f**, **h**, **n**, **o**). $^*P < 0.05$, $^{***}P < 0.001$.

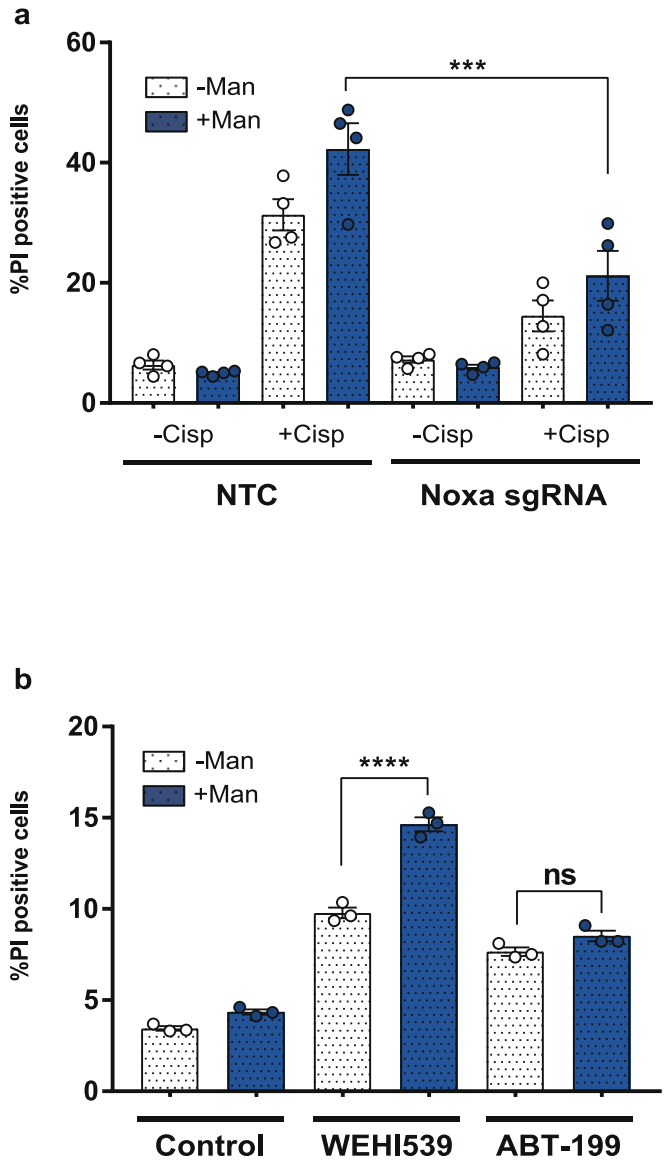

Extended Data Fig. 5 | Sensitization to cell death by mannose is connected to Bcl-2 family members. a, Percentage of control (NTC) and *Noxa* CRISPR U2OS-E1a propidium-iodide-positive cells upon 24 h treatment with or without 10 μM cisplatin and with or without 25 mM mannose. **b**, Percentage of U2OS-E1a propidium-iodide-positive cells upon 24 h treatment with 10 μM WEHI539 (a $BclX_L$ inhibitor) or 10 μM ABT-199 (a Bcl-2 inhibitor), with or without 25 mM mannose. $n = 4$ independent experiments (**a**); $n = 3$ three independent experiments (**b**). All data are mean ± s.e.m. and were analysed by two-way ANOVA with Bonferroni correction (**a**) and two-tailed unpaired *t*-test (**b**). ***$P < 0.001$; ****$P < 0.0001$; NS, not significant.

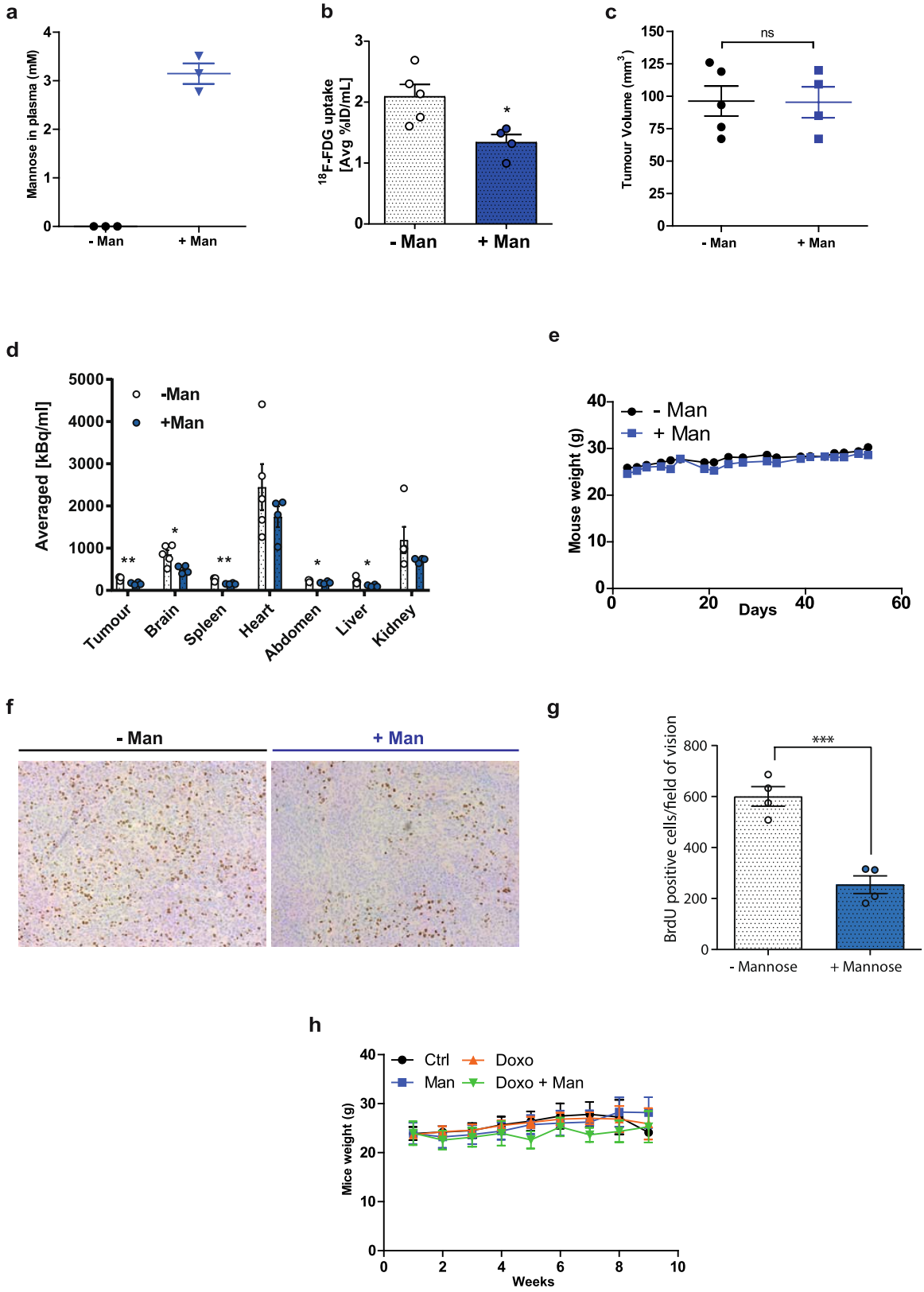

Extended Data Fig. 6 | See next page for caption.

Extended Data Fig. 6 | Mannose affects cell proliferation and the uptake/retention of ^{18}F-FDG, but it does not affect animal weight. **a**, Mannose levels in the plasma after 60 min in mice treated with a single dose of 200 μl water or 20% mannose in water. **b**, **c**, CD1-nude mice were transplanted with KP-4 cells subcutaneously and tumours were grown for 14 days. PET and MRI scans were performed for mice treated with 200 μl of water or 20% mannose in water by oral gavage 20 min before injection of [^{18}F]FDG into the tail vein. **b**, Quantification of [^{18}F]FDG uptake by tumours represented in average percentage injected dose per ml (%ID ml^{-1}) ± s.d. **c**, Volume of each tumour at the time of the PET and MRI scans. Data were analysed by unpaired two-tailed Student's *t*-test. **d**, CD1-nude mice were injected with KP-4 cells subcutaneously and treated with normal drinking water or 20% mannose in the drinking water, plus the same treatment (either normal water or 20% mannose) by oral gavage three days a week from the third day after tumour transplantation. Shown is the quantification of [^{18}F]FDG uptake by the tumour and different organs represented in averaged kBq ml^{-1} ± s.d. Data were analysed by unpaired two-tailed Student's *t*-test. **e**, CD1-nude mice were injected with KP-4 cells subcutaneously and treated with normal drinking water or 20% mannose in the drinking water, plus the same treatment (either normal water or 20% mannose) by oral gavage three days a week from the third day after tumour transplantation. The weight of mice was recorded at the indicated times. **f**, **g**, CD1-nude mice were injected with KP-4 cells subcutaneously and treated with normal drinking water or 20% mannose in the drinking water (either normal water or 20% mannose) by oral gavage three days a week from the third day after tumour transplantation. **f**, Images of BrdU sections representing tumours in control (left) and mannose-treated (right) mice. **g**, Quantification of BrdU-positive cells per section in control tumours ($n = 4$) and mannose-treated ($n = 4$) tumours. Five representative images per tumour were analysed. **h**, CD1-nude mice were injected with KP-4 cells subcutaneously and tumours were grown for 10 days before treatment with mannose and/or doxorubicin (doxo) was started. Mice received normal drinking water (ctrl and doxo) or 20% mannose in the drinking water (man and doxo + man) together with the same treatment by oral gavage three times per week. Doxorubicin treatment started on day 32 and mice received 5 mg kg^{-1} by intraperitoneal injection once per week. The weight of mice in all groups was recorded throughout the experiment. The number of mice for each experiment is as follows: $n = 3$ per group (**a**), $n = 5$ (−mannose), $n = 4$ (+mannose) (**b**–**d**); $n = 10$ (**h**). In **a**, **c** and **h** data are mean ± s.e.m. Data were analysed with a two-tailed unpaired *t*-test (**c**). $^{*}P < 0.05$, $^{**}P < 0.01$.

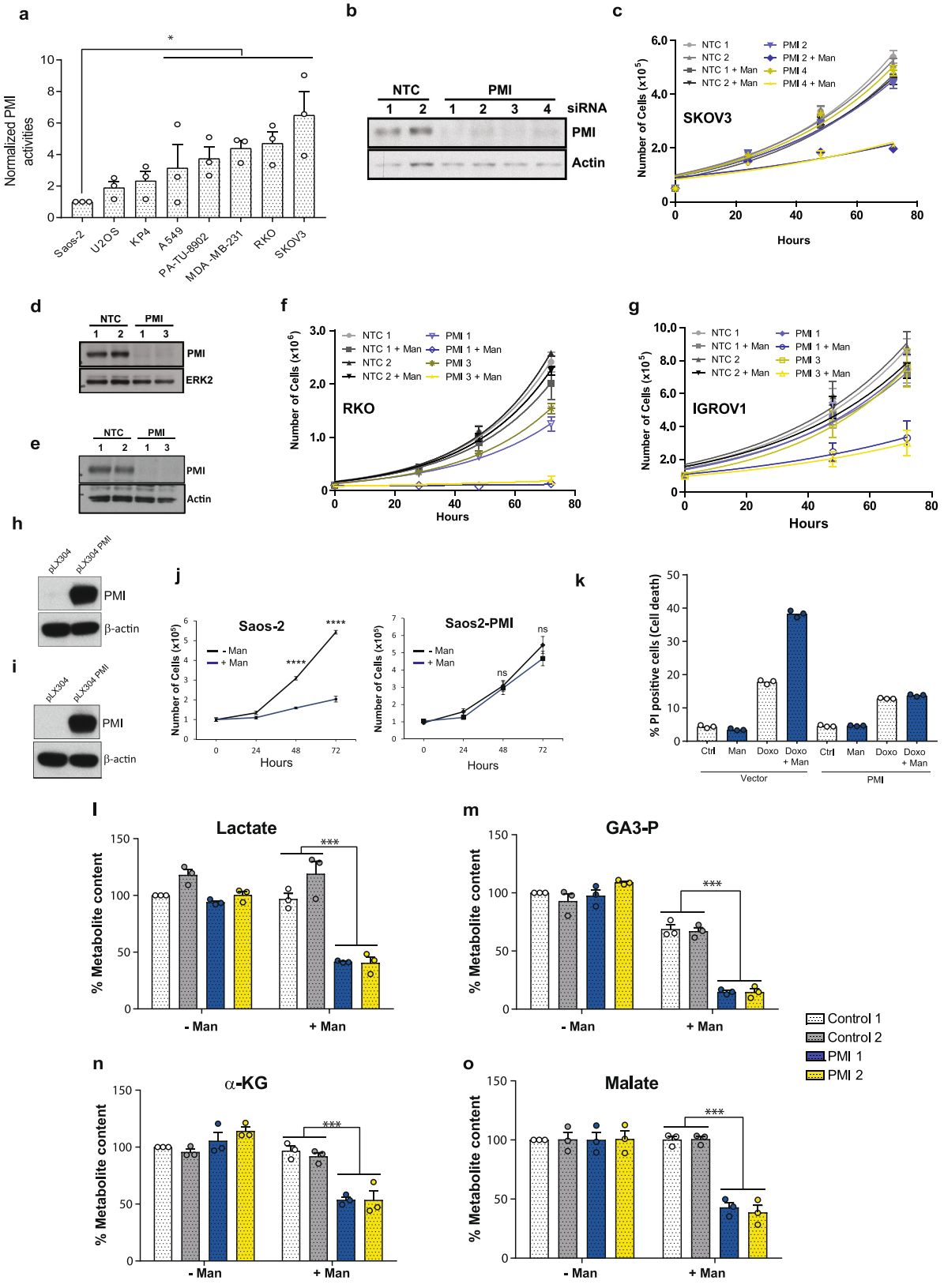

Extended Data Fig. 7 | See next page for caption.

Extended Data Fig. 7 | PMI levels dictate the response to mannose. **a**, PMI expression levels correlate with PMI activities. PMI activities were measured in eight different cell lines using coupled enzymatic reactions. Graph shows the OD_{340nm} measured at 2 h, reflecting the amount of $NADPH/H^+$ produced by the reactions. Results from three independent experiments were normalized relative to PMI activities measured in Saos-2 cells and represent mean ± s.e.m. **b**–**g**, *MPI* knockdown sensitizes cells to mannose. **b**, Western blot of SKOV3-transfected cells showing the levels of PMI and actin after 48 h of transient transfection with siRNAs. Growth curves of SKOV3 (**c**), RKO (**f**) and IGROV1 (**g**) in regular DMEM supplemented with or without 25 mM mannose after transient transfection for 48 h with two NTC and two *MPI*-targeting siRNAs. **d**, **e**, Western blot showing the levels of PMI and ERK2 in RKO (**d**) and PMI and actin in IGROV1 (**e**) 48 h after siRNA transfection. **h**–**k**, Overexpression of PMI causes resistance to the growth-suppressing and death-promoting effects of mannose. PMI expression in U2OS-E1a (**h**) and Saos-2 (**i**) cells was confirmed by western blotting. **j**, Saos2-PMI cells and control cells (Saos-2) were plated in the presence or the absence of 25 mM mannose and cell numbers were counted at the indicated times. **k**, Percentage of propidium-iodide-positive U2OS-E1a control cells (vector) or U2OS-E1a cells overexpressing PMI (PMI) after 24 h treatment with or without 1 $\mu g\ ml^{-1}$ doxorubicin in the presence or absence of 25 mM mannose. **l**–**o**, Percentage of lactate (**l**), GA3-P (**m**), α-KG (**n**) and malate (**o**) metabolite content (peak area) in SKOV3 cells transfected with siRNA for 48 h before 6 h incubation in complete DMEM medium with or without supplementation of 25 mM mannose. $n = 3$ independent experiments (**a**, **c**, **f**, **g**, **j**, **l**–**o**). Data are representative of two independent experiments (**b**, **d**, **e**, **k**), or one experiment (**h**, **i**). Data are mean ± s.e.m. and were analysed by two-tailed unpaired *t*-test (**a**), two-way ANOVA with Tukey correction (**l**–**o**) or multiple unpaired two-sided *t*-test with Holm–Sidak correction (**j**). $^*P < 0.05$, $^{***}P < 0.001$, $^{****}P < 0.0001$.

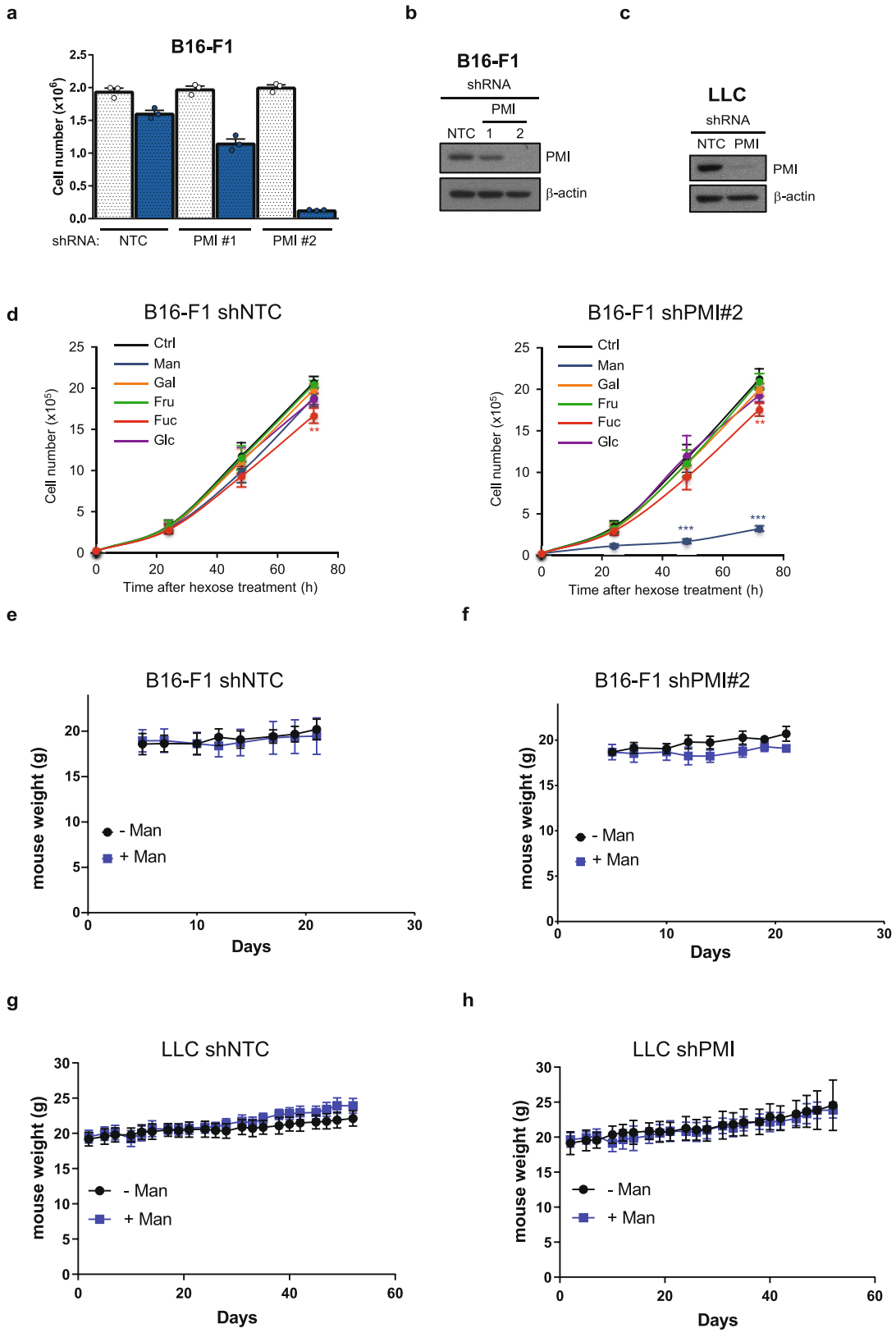

Extended Data Fig. 8 | See next page for caption.

Extended Data Fig. 8 | PMI levels dictate mannose sensitivity, and the weight of animals containing syngeneic allografts is not affected by treatment with mannose. a, **b**, *Mpi* knockdown causes growth retardation upon mannose treatment in a dose-dependent manner. **a**, B16-F1 cells infected with NTC or shRNA against *Mpi* were treated with (blue columns) or without (white columns) 25 mM mannose for 72 h, after which the number of cells was determined. Data are mean ± s.e.m. $n = 3$ independent experiments. **b**, The reduction in PMI was confirmed by western blotting. **c**, Western blot showing a reduction in PMI after *Mpi* knockdown in LLC cells. The data are relative to the experiments shown in Fig. 4g, j, k. **d**, B16-F1 cells infected with NTC or shRNA against *Mpi* were treated with 25 mM mannose, 25 mM glucose, 25 mM galactose, 25 mM fructose or 25 mM fucose. At 24, 48 and 72 h after hexose treatment, the number of cells was determined. Data are mean ± s.e.m. **e**–**h**, Weights of mice injected with syngeneic cell lines: B16 shNTC (**e**), B16 shPMI (**f**), LLC shNTC (**g**) and LLC shPMI (**h**); the mice were given normal drinking water or drinking water supplemented with 20% mannose ($n = 10$ mice per group). All data are mean ± s.d. unless otherwise stated. In **d**, $n = 4$ independent experiments were analysed by two-way ANOVA followed by Tukey's multiple comparisons. The data in **b** and **c** were performed only once. $^{***}P < 0.001$.

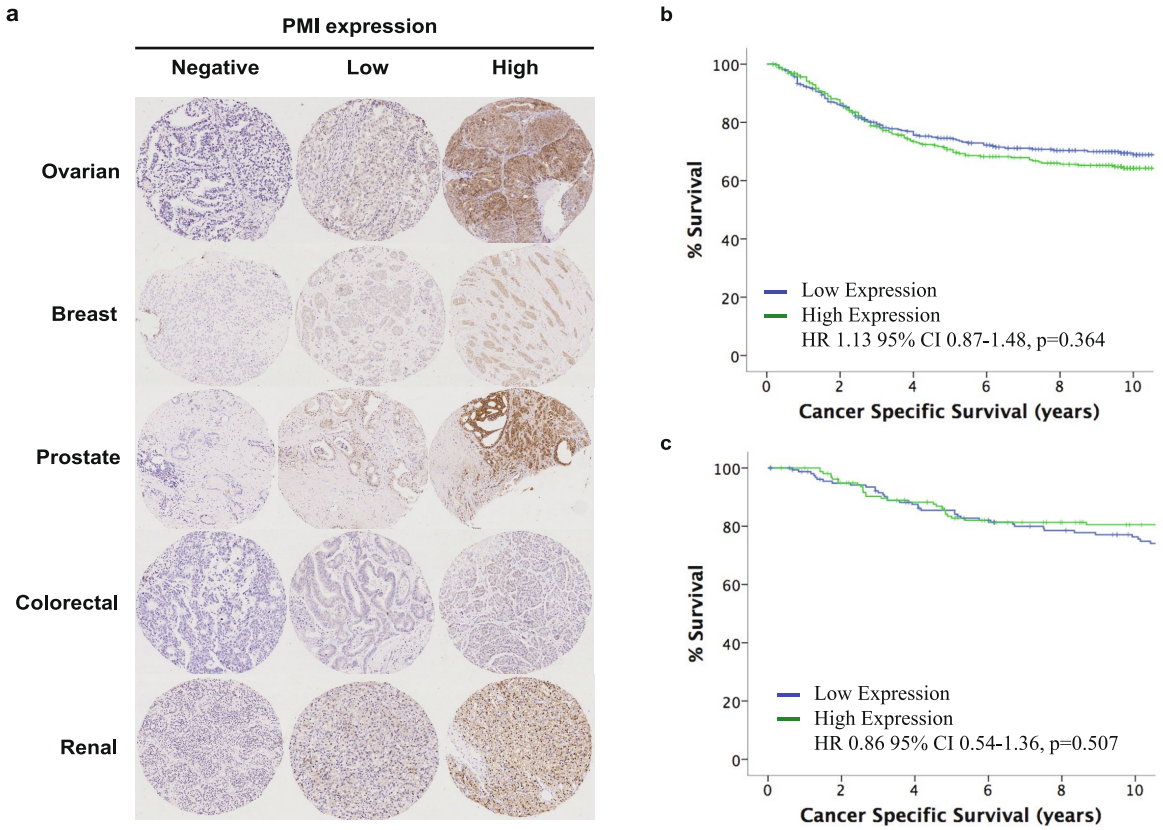

d

	Colorectal Cancer (n=698)			Breast Cancer (n=316)		
	N (%)	10yr CSS (SE)	*P*	*N (%)*	10yr CSS (SE)	*P*
Cytoplasmic PMI (n=698)			0.364			0.507
Low expression	347 (50)	69 (3)		157 (50)	76 (4)	
High expression	351 (50)	64 (3)		159 (50)	81 (3)	

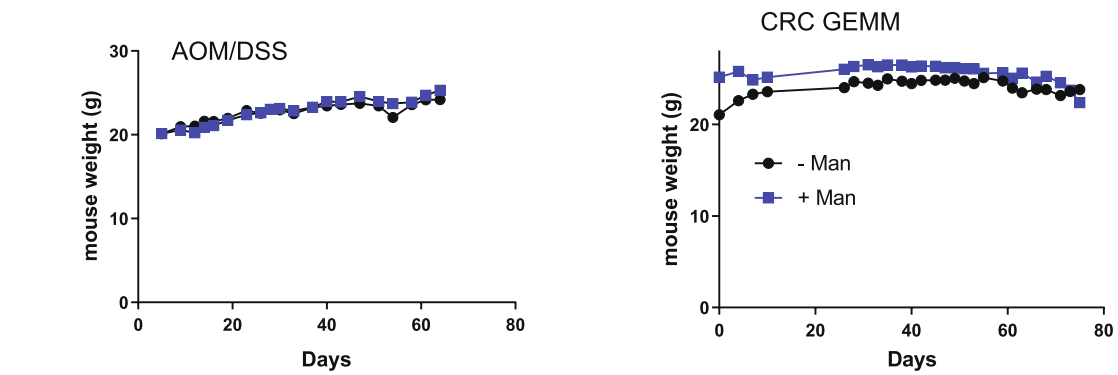

Extended Data Fig. 9 | PMI levels vary in human tumours, but do not predict overall survival and the weight of mice is not affected by mannose treatment in models of colorectal cancer. a, Images of PMI expression for each TMA, representing one negative sample (left), one low expression (middle) and one high expression (right). One sample came from each of the ovarian, breast, prostate, colorectal or renal TMAs as indicated. **b**, **c**, Kaplan–Meier curves showing cancer-specific survival based on PMI levels in $n = 698$ patients with stage I–IV colorectal cancer (**b**) or $n = 316$ patients with primary operable breast cancer (**c**). **d**, Table showing the association of PMI and cancer-specific survival. Histoscores were split into high and low expression using the ROC curve analysis for each tumour type. log-rank analysis (two-sided) was used to compare PMI and cancer-specific survival using SPSS (version 22). **e**, Mean weight of 28 mice during treatment with AOM and DSS, with or without additional mannose treatment. **f**, Weight of aged *Villin*^{creER}*Apc*$^{fl/+}$*Kras*$^{G12D/+}$ mice during treatment with or without mannose. Data are mean of each group ($n = 7$ mice, −mannose; $n = 8$ mice, +mannose).

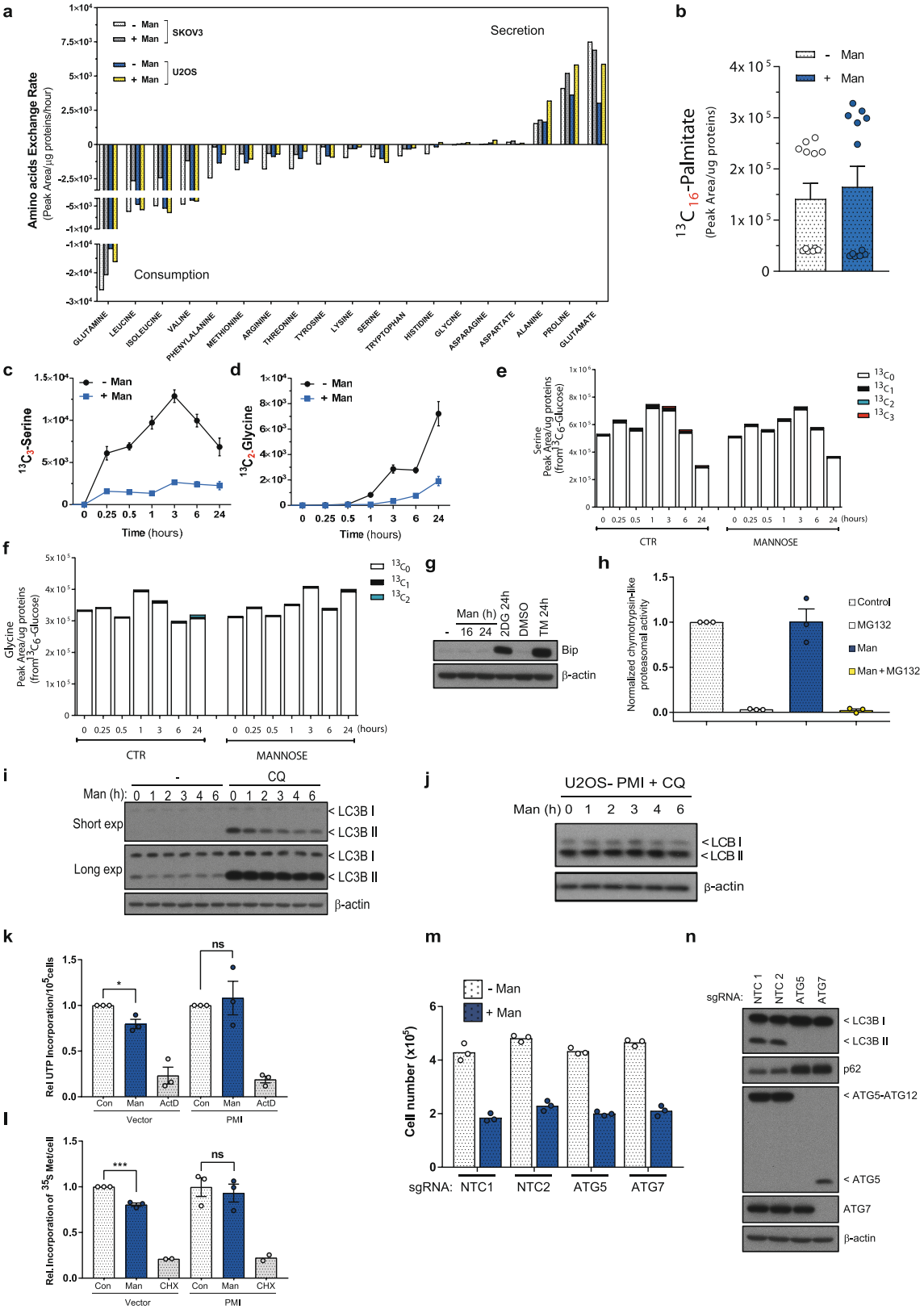

Extended Data Fig. 10 | See next page for caption.

Extended Data Fig. 10 | Mannose does not affect amino acid and fatty acid uptake, nor does it significantly affect serine and glycine levels, endoplasmic reticulum stress or proteasome activity, but it does affect autophagy, transcription and translation in a PMI-dependent manner. **a**, Exchange rates of amino acids between the indicated cells and their media measured after 48 h treatment with or without 25 mM mannose. Results are presented as peak area per microgram of protein per hour and are representative of one experiment. Shown is the mean of six technical replicates. **b**, Levels of $^{13}C_{16}$-palmitate (expressed as peak area per microgram of protein) in U2OS-E1a cells incubated with 50 μM $^{13}C_{16}$-palmitate, conjugated with 10% fatty-acid-free BSA, for 24 h in the presence or absence of 25 mM mannose in the culture medium (DMEM). $n = 2$ independent experiments (each involving six technical replicates). Data are mean ± s.e.m. **c**, **d**, Levels of $^{13}C_3$-serine (**c**) and $^{13}C_2$-glycine (**d**) (expressed as peak area per micrograms of protein) in U2OS-E1a cells incubated with 25 mM $^{13}C_6$-glucose for the indicated time in the presence or absence of 25 mM mannose in the culture medium (DMEM). $n = 3$ independent experiments. **e**, **f**, Distribution of isotopologues of intracellular serine (**e**) and glycine (**f**) in U2OS-E1a cells incubated with 25 mM $^{13}C_6$-glucose for 24 h in the presence (mannose) or absence (ctr) of 25 mM mannose in the culture medium (DMEM). $n = 3$ independent experiments. **g**, Mannose has no effect on the unfolded protein response. U2OS-E1a cells were treated with 25 mM mannose for 16 and 24 h. 2-Deoxy-D-glucose (2DG) and tunicamycin (TM) serve as positive controls. Induction of Bip (also known as GRP78) is a read-out of endoplasmic reticulum stress. The data are representative of three independent experiments. **h**, Proteasome activity is not affected by mannose. Mannose-sensitive U2OS-E1a cells were incubated in either DMEM or DMEM containing 25 mM mannose before measurement of proteasome activities. Cells were also treated with10 μM MG132 as a control for proteasome activity. $n = 3$ independent experiments. **i**, **j**, U2OS-E1a cells (**i**) or U2OS-E1a (U2OS) cells overexpressing PMI (**j**) were treated with 25 mM mannose for the indicated times in the presence or absence of 20 μM chloroquine (CQ) (4 h). Western blotting was undertaken to detect LC3-B and actin. The data are representative of three independent experiments. **k**, **l**, Relative incorporation of ^{32}P UTP (**k**) or ^{35}S methionine (**l**) into U2OS-E1a control cells (vector) or U2OS-E1a cells overexpressing PMI (PMI) in the presence or absence of 25 mM mannose. Where indicated, 5 μM actinomycin D was used to inhibit transcription or 100 μg ml^{-1} cycloheximide was used to inhibit translation. In **k**, $n = 3$ independent experiments. In **l**, $n = 3$ independent experiments (control and mannose) and $n = 2$ independent experiments (CHX). **m**, **n**, U2OS-E1a cells infected with lentiCRISPR-NTC 1, NTC 2, ATG5 or ATG7 were treated with 25 mM D-(+)-mannose for 72 h. **m**, The number of cells counted after the 72-h treatment; the results represent the mean of one independent experiment performed in triplicate. **n**, Western blots show loss of LC3 lipidation and p62 accumulation in *ATG5* and *ATG7* knockout cells. Data were analysed by two-tailed unpaired *t*-tests. $*P < 0.05$, $***P < 0.001$. Unless otherwise stated, data are mean ± s.e.m.

nature research

Corresponding author(s): Kevin M. Ryan

Reporting Summary

Nature Research wishes to improve the reproducibility of the work that we publish. This form provides structure for consistency and transparency in reporting. For further information on Nature Research policies, see Authors & Referees and the Editorial Policy Checklist.

Statistical parameters

When statistical analyses are reported, confirm that the following items are present in the relevant location (e.g. figure legend, table legend, main text, or Methods section).

n/a	Confirmed	
☐	☒	The exact sample size (*n*) for each experimental group/condition, given as a discrete number and unit of measurement
☐	☒	An indication of whether measurements were taken from distinct samples or whether the same sample was measured repeatedly
☐	☒	The statistical test(s) used AND whether they are one- or two-sided *Only common tests should be described solely by name; describe more complex techniques in the Methods section.*
☒	☐	A description of all covariates tested
☐	☒	A description of any assumptions or corrections, such as tests of normality and adjustment for multiple comparisons
☐	☒	A full description of the statistics including central tendency (e.g. means) or other basic estimates (e.g. regression coefficient) AND variation (e.g. standard deviation) or associated estimates of uncertainty (e.g. confidence intervals)
☐	☒	For null hypothesis testing, the test statistic (e.g. *F*, *t*, *r*) with confidence intervals, effect sizes, degrees of freedom and *P* value noted *Give P values as exact values whenever suitable.*
☒	☐	For Bayesian analysis, information on the choice of priors and Markov chain Monte Carlo settings
☒	☐	For hierarchical and complex designs, identification of the appropriate level for tests and full reporting of outcomes
☒	☐	Estimates of effect sizes (e.g. Cohen's *d*, Pearson's *r*), indicating how they were calculated
☐	☒	Clearly defined error bars *State explicitly what error bars represent (e.g. SD, SE, CI)*

Our web collection on statistics for biologists may be useful.

Software and code

Policy information about availability of computer code

Data collection	Data was collected on Applied Biosystems StepOnePlus PCR system using StepOne software version 2.3 (qPCR), , Thermo Fisher Exactive Orbitrap using Thermo Fisher Xcalibur software version 2.2 for aquisition (Mass Specrometry) and BD Biosciences Facscalibur and ATTune NXT flow cytometer (Flow cytometry).
Data analysis	Data analysis was undertaken using Microsoft Excel 2010, Graphpad Prism version 7, PMOD version 3.504, Thermo TraceFinder (version 3.2), SPSS version 22.

For manuscripts utilizing custom algorithms or software that are central to the research but not yet described in published literature, software must be made available to editors/reviewers upon request. We strongly encourage code deposition in a community repository (e.g. GitHub). See the Nature Research guidelines for submitting code & software for further information.

Data

Policy information about availability of data

All manuscripts must include a data availability statement. This statement should provide the following information, where applicable:

- Accession codes, unique identifiers, or web links for publicly available datasets
- A list of figures that have associated raw data
- A description of any restrictions on data availability

Data that support the findings in this study are stored at the Cancer Research UK Beatson Institute and are available from the corresponding author upon reasonable request.

Field-specific reporting

Please select the best fit for your research. If you are not sure, read the appropriate sections before making your selection.

☒ Life sciences ☐ Behavioural & social sciences ☐ Ecological, evolutionary & environmental sciences

For a reference copy of the document with all sections, see nature.com/authors/policies/ReportingSummary-flat.pdf

Life sciences study design

All studies must disclose on these points even when the disclosure is negative.

Sample size	Experimental group/cohort sizes were based on previous similar studies that have given statistical results. For animals this also respected the limited use of animals in line with the 3R system: Replacement, Reduction, Refinement.
Data exclusions	No data were excluded.
Replication	Where replication is indicated in the manuscript, the attempts at replication were successful.
Randomization	For animal treatments, all studies were randomized.
Blinding	Yes, this was done for the Tissue Microarray (IHC) scoring.

Reporting for specific materials, systems and methods

Materials & experimental systems

n/a	Involved in the study
☐	☒ Unique biological materials
☐	☒ Antibodies
☐	☒ Eukaryotic cell lines
☒	☐ Palaeontology
☐	☒ Animals and other organisms
☒	☐ Human research participants

Methods

n/a	Involved in the study
☒	☐ ChIP-seq
☐	☒ Flow cytometry
☐	☒ MRI-based neuroimaging

Unique biological materials

Policy information about availability of materials

Obtaining unique materials	The majority of materials are commercially available and materials generated by us will be available upon request.

Antibodies

Antibodies used	The following antibodies were used at a 1/1000 dilution unless otherwise stated: β-Actin (Abcam; ab8227), Mcl-1 (Cell signaling; 4572), ERK2 (Santa Cruz; sc-154), Bcl-XL (Cell signaling; 2762), HSP-90β (Santa Cruz; sc-1057), PARP (Cell signalling; 9542), Cleaved-caspase-3 (Cell signalling; 9664), FADD (Transduction labs; F36620), Caspase-8 (Cell signalling; 4790), Bax (Transduction labs; 610983), Bak (Cell signalling; 6947), Bim (Cell signalling; 2993), Noxa (Novus Biologicals; NB-600-1159), phospho-AMPKα (Cell signalling; 2535), AMPKα (Cell signalling; 5832), PMI (Abcam; 128115). LC3B (Cell Signaling Technology, Cat#: 2775S,

	1/1500), ?-actin (Cell Signaling Technology, Cat#: 4670S, 1/2000), ATG5 (Cell Signaling Technology, Cat#: 12994S), ATG7 (Cell Signaling Technology, Cat#: 8558S), Bip/GRP78 (Cell Signaling Technology, Cat#: 3177S), p62 (BD Biosciences, Cat#: 610833, 1/2000). Mouse PMI protein was detected using rabbit polyclonal PMI antibody (Proteintech, Cat#: 14234-1-AP). BrdU (BD Biosciences #347580) was used for immunohistochemistry at 1/200 dilution.
Validation	Validation was based on information provided in manufacturers' datasheets. In addition, as indicated in the manuscript, we utilized RNAi or CRISPR/Cas9 to validate the following the antibodies used to detect the following proteins: Bax, Bak, Caspase-8, FADD, PMI, Atg5 and Atg7.

Eukaryotic cell lines

Policy information about cell lines

Cell line source(s)	Cell lines were originally from ATCC, ECACC, DMSZ or RIKEN and are drawn from stocks at the Cancer Research UK Beatson Institute
Authentication	The cell lines were not recently authenticated.
Mycoplasma contamination	All cell lines are routinely tested for mycoplasma and it is considered that the lines used in the study are mycoplasma free.
Commonly misidentified lines (See ICLAC register)	No commonly misidentified lines were used in the study.

Animals and other organisms

Policy information about studies involving animals; ARRIVE guidelines recommended for reporting animal research

Laboratory animals	Mice used in this study were 6-week old female CD1-nude mice (xenografts), 6-week old female C57/BL6J wild-type mice (allografts and AOM/DSS and 6-12 week old male and female C57/BL6J).
Wild animals	No wild animals were used in this study.
Field-collected samples	No field-collected samples were used in this study.

Flow Cytometry

Plots

Confirm that:

☒ The axis labels state the marker and fluorochrome used (e.g. CD4-FITC).

☒ The axis scales are clearly visible. Include numbers along axes only for bottom left plot of group (a 'group' is an analysis of identical markers).

☐ All plots are contour plots with outliers or pseudocolor plots.

☒ A numerical value for number of cells or percentage (with statistics) is provided.

Methodology

Sample preparation	A citation describing sample preparation in included in the Methods section
Instrument	Becton Dickinson FACSCalibur and Life Technologies ATTune NXT
Software	CellQuest and FlowJo version 10
Cell population abundance	No sorting was conducted.
Gating strategy	FSC/SSC were used to discern single cells from doublets/multiple cells. Samples without flourescent staining were used to establish boundaries between negative and positive cells.

☐ Tick this box to confirm that a figure exemplifying the gating strategy is provided in the Supplementary Information.

Magnetic resonance imaging

Experimental design

Design type	Sequential PET and MRI scans were performed in same session on a dual-modality PET/MRI scanner. MRI scans were performed to obtain anatomical reference for the quantification of positron emission tomography (PET) images.
Design specifications	For each mouse, static PET acquisitions were performed for 15 min and after that whole body T1-weighed GRE 3D

Design specifications	Multi-FOV MRI scans (~22 min) performed to obtain anatomical references.
Behavioral performance measures	N/A

Acquisition

Imaging type(s)	Structural type: To obtain anatomical reference for positron emission tomography (PET) scans
Field strength	1 Tesla
Sequence & imaging parameters	T1-weighed Echo Gradient Echo Sequence (GRE) 3D Multi-field-of-view (FOV) MRI Slice thickness 0.50mm Repetition time (TR) 10msec Echo time (TE) 2.3msec Flip angle 12 degrees
Area of acquisition	Whole body scans were performed. Whole body region was selected by a quick Scout (a fast GRE-based sequence) scan for localization in <2 min.

Diffusion MRI ☐ Used ☒ Not used

Preprocessing

Preprocessing software	For MRI scan acquisition- Mediso Nucline NanoScan version v2.01 (Build 019.0000) For PET/MRI image analysis- PMOD software version 3.504 (PMOD Technologies Ltd.)
Normalization	No normalization was performed for MRI scans. However, normalization/ quantification was performed for PET images.
Normalization template	N/A
Noise and artifact removal	N/A
Volume censoring	N/A

Statistical modeling & inference

Model type and settings	N/A
Effect(s) tested	N/A

Specify type of analysis: ☐ Whole brain ☒ ROI-based ☐ Both

Anatomical location(s)	MRI scans were not quantified. For quantitative assessments of PET scans, ROI were manually drawn around the edge of the tumour xenograft on MRI scans by visual inspection using PMOD software version 3.504 (PMOD Technologies Ltd.) and same ROI copied on respective PET scans for quantification.
Statistic type for inference (See Eklund et al. 2016)	MRI scans were not quantified.
Correction	N/A

Models & analysis

n/a	Involved in the study
☒	☐ Functional and/or effective connectivity
☒	☐ Graph analysis
☒	☐ Multivariate modeling or predictive analysis